

LUND UNIVERSITY

III-V Nanowire Solar Cells: Growth and Characterization

Otnes, Gaute

2018

Document Version:
Publisher's PDF, also known as Version of record

Link to publication

Citation for published version (APA):
Otnes, G. (2018). *III-V Nanowire Solar Cells: Growth and Characterization*. Department of Physics, Lund University.

Total number of authors:
1

Creative Commons License:
Other

General rights
Unless other specific re-use rights are stated the following general rights apply:
Copyright and moral rights for the publications made accessible in the public portal are retained by the authors and/or other copyright owners and it is a condition of accessing publications that users recognise and abide by the legal requirements associated with these rights.
• Users may download and print one copy of any publication from the public portal for the purpose of private study or research.
• You may not further distribute the material or use it for any profit-making activity or commercial gain
• You may freely distribute the URL identifying the publication in the public portal

Read more about Creative commons licenses: https://creativecommons.org/licenses/

Take down policy
If you believe that this document breaches copyright please contact us providing details, and we will remove access to the work immediately and investigate your claim.

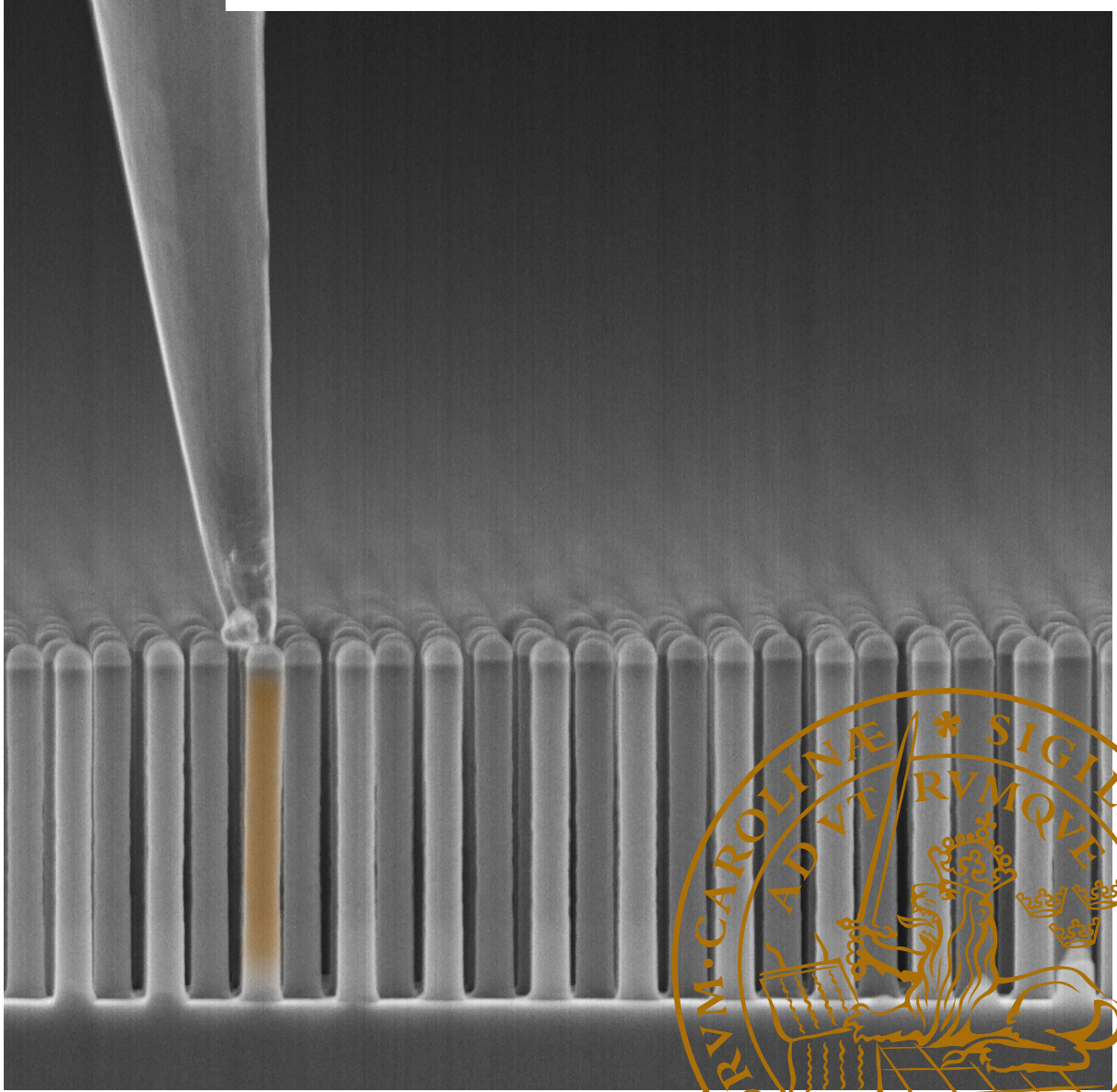
LUND UNIVERSITY

PO Box 117
221 00 Lund
+46 46-222 00 00

Download date: 02. Nov. 2026

III-V Nanowire Solar Cells: Growth and Characterization

GAUTE OTNES
DIVISION OF SOLID STATE PHYSICS | LUND UNIVERSITY



III-V Nanowire Solar Cells: Growth and Characterization

Gaute Otnes



LUND
UNIVERSITY

DOCTORAL DISSERTATION
by due permission of the Faculty of Engineering, Lund University, Sweden.
To be defended on Friday, March 16th, 2018 at 09:15 in Rydbergsalen,
Sölvegatan 14, Lund, for the degree of Doctor of Philosophy in Engineering.

Faculty opponent
Professor Sarah Kurtz
University of California, Merced/National Renewable Energy Laboratory

Organization LUND UNIVERSITY	Document name DOCTORAL DISSERTATION
	Date of issue
Author Gaute Otnes	Sponsoring organization

Title: III-V Nanowire Solar Cells: Growth and Characterization

Abstract

To mitigate dangerous climate change, a transition to a new and sustainable energy system is needed. In this system, solar energy will need to be a key player. Prices of electricity made from solar cells have declined rapidly over the recent decades, making solar energy competitive in more markets. However, further price reductions and new innovations are needed for solar cell technology to fulfil its potential.

In this thesis, we look at a class of materials that have gained increasing interest in the recent decade; III-V semiconductor nanowires. For solar cells, the III-V semiconductors hold excellent optical and electrical properties, but high material and manufacturing costs have so far prevented competitiveness with the dominating Si-based technology. However, III-V material in the nanowire geometry has a number of interesting advantages when it comes to reducing cost, as well as for adding III-Vs to conventional Si in tandem solar cell architectures. This has motivated substantial research efforts during recent years, both at universities and private companies.

In this thesis, we have mainly studied InP and $In_xGa_{1-x}P$ nanowire arrays as a solar cell material. The nanowires were grown by metal organic vapor phase epitaxy (MOVPE) via gold seeded vapor-liquid-solid growth. The gold seed particles were placed in a pattern on the growth substrate by help of nanoimprint lithography. Developing strategies to preserve this pattern through the stages of nanowire growth was an important foundation for the thesis work. These strategies allowed us to reproducibly grow dense and ordered arrays of nanowires, optimized for sunlight absorption.

Controllably changing the electrical properties of the semiconductor through impurity doping is important to make a good solar cell. Doping nanowires is challenging since the growth mechanism is different from established layer growth by MOVPE, and nanowire characterization is demanding. We have studied doping in our nanowires in various ways. Most importantly, we have performed some of the first systematic doping studies in ternary III-V materials, with bandgaps needed to create tandem nanowire solar cells. Knowledge from these studies allowed us to realize and study the first nanowire tunnel junction connecting two materials of appropriate bandgap to match the solar spectrum

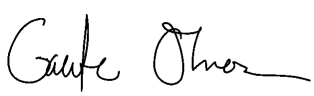
Finally, we have developed a characterization procedure to optimize nanowire solar cell characteristics. This helped us create a better understanding of performance limiting factors in our InP nanowire solar cells. As a result, we achieved more than a sevenfold performance improvement in these cells, with the best device having a certified power conversion efficiency of 15.0%. This is currently the highest reported efficiency value for a bottom-up synthesized InP nanowire solar cell.

Key words: Solar cell, nanowire, III-V, semiconductor, photovoltaics, epitaxy, lithography, characterization

Classification system and/or index terms (if any)

Supplementary bibliographical information		Language: English
ISSN and key title		ISBN 978-91-7753-565-2
Recipient's notes	Number of pages	Price
	Security classification	

I, the undersigned, being the copyright owner of the abstract of the above-mentioned dissertation, hereby grant to all reference sources permission to publish and disseminate the abstract of the above-mentioned dissertation.

Signature  Date 2018-02-05

III-V Nanowire Solar Cells: Growth and Characterization

Gaute Otnes



LUND
UNIVERSITY

Front cover: Scanning electron microscope image of an InP nanowire array grown from gold particles defined by nanoimprint lithography. One nanowire is contacted by a tungsten nanoprobe, and colorized to indicate the electron beam induced current signal.

Copyright 2018 Gaute Otnes, pp. i-xx, 1-56.

Division of Solid State Physics
Department of Physics
Lund University
SE-221 00 Lund
Sweden

ISBN 978-91-7753-565-2 (print)
ISBN 978-91-7753-566-9 (electronic)

Printed in Sweden by Media-Tryck, Lund University
Lund 2018





MADE IN SWEDEN

Media-Tryck is an environmentally certified and ISO 14001 certified provider of printed material. Read more about our environmental work at www.mediatryck.lu.se

Table of Contents

Abstract vii
Popular Science Summary ix
Acknowledgements xiii
List of Papers xvii

1 Introduction 1
1.1 Thesis outline 3

2 Nanowire solar cells 5
2.1 Solar cell basics 5
2.2 Benefits of the nanowire geometry 15
2.3 Design of a nanowire solar cell 16

3 Nanowire array synthesis 19
3.1 Metal organic vapor phase epitaxy 19
3.2 Basics of particle seeded nanowire growth 25
3.3 Growth substrates 28
3.4 Some growth considerations for nanowire solar cells 33

4 Characterization 39
4.1 In situ optical reflectometry 39
4.2 Scanning electron microscopy 41
4.3 Doping evaluation 42
4.4 Electron beam induced current 43
4.5 Solar cell *IV*-characteristics 45

5 Summary and outlook 47

References 49

Abstract

To mitigate dangerous climate change, a transition to a new and sustainable energy system is needed. In this system, solar energy will need to be a key player. Prices of electricity made from solar cells have declined rapidly over recent decades, making solar energy competitive in more markets. However, further price reductions and new innovations are needed for solar cell technology to fulfil its potential.

In this thesis, we look at a class of materials that have gained increasing interest in the recent decade; III-V semiconductor nanowires. For solar cells, the III-V semiconductors hold excellent optical and electrical properties, but high material and manufacturing costs have so far prevented competitiveness with the dominating Si-based technology. However, III-V material in the nanowire geometry has a number of interesting advantages when it comes to reducing cost, as well as for adding III-Vs to conventional Si in tandem solar cell architectures. This has motivated substantial research efforts during recent years, both at universities and private companies.

In this thesis, we have mainly studied InP and $In_xGa_{1-x}P$ nanowire arrays as a solar cell material. The nanowires were grown by metal organic vapor phase epitaxy (MOVPE) via gold seeded vapor-liquid-solid growth. The gold seed particles were placed in a pattern on the growth substrate by help of nanoimprint lithography. Developing strategies to preserve this pattern through the stages of nanowire growth was an important foundation for the thesis work. These strategies allowed us to reproducibly grow dense and ordered arrays of nanowires, optimized for sunlight absorption.

Controllably changing the electrical properties of the semiconductor through impurity doping is important to make a good solar cell. Doping nanowires is challenging since the growth mechanism is different from established layer growth by MOVPE, and nanowire characterization is demanding. We have studied doping in our nanowires in various ways. Most importantly, we have performed some of the first systematic doping studies in ternary III-V materials, with bandgaps needed to create tandem nanowire solar cells. Knowledge from these studies allowed us to realize and study the first nanowire tunnel junction connecting two materials of appropriate bandgap to match the solar spectrum.

Finally, we have developed a characterization procedure to optimize nanowire solar cell characteristics. This helped us create a better understanding of performance limiting factors in our InP nanowire solar cells. As a result, we achieved more than a sevenfold performance improvement in these cells, with the best device having a certified power conversion efficiency of 15.0%. This is currently the highest reported efficiency value for a bottom-up synthesized InP nanowire solar cell.

Popular Science Summary

To limit dangerous climate change while providing energy to a growing world population, a massive build-up of renewable energy technologies will be needed throughout the coming decades. Using solar cells to produce electricity directly from the energy contained in sunlight is one of the most important pieces of this puzzle, simply due to its abundance; if we could harvest all the energy from the sunlight striking the Earth, less than two hours would be enough to cover the world's energy need for an entire year.

The global solar cell production capacity has increased enormously over the last two decades, growing by around 40% per year. Economy of scale and continuous technological development has led to a steady decline in the price of solar cell electricity, driven by political support in Germany and other countries. As a result, the technology has become competitive in more and more markets. However, solar energy as of 2017 still only contributes to around 2% of the global electricity production. To make solar energy fulfill its potential as a major contributor in the new sustainable energy system, continued innovation and technological development is needed.

To understand the challenges in improving solar cell technology, it is useful to start by discussing two of the main challenging factors in solar energy harvesting. The first one is that while the energy from the Sun is abundant, it is spread out over a large area (the half of the Earth which is illuminated at any given time). This means that any technology used to harvest solar energy needs to be very cheap, to cover enough area in a cost-effective manner.

The second challenging factor comes from the solar energy being distributed between all the different wavelengths coming from the Sun; some of the energy comes in the form of ultraviolet light (the invisible part of the sunlight which causes skin cancer), the largest part as visible light (light of the different colors in the rainbow) and also a significant part as infrared light (heat radiation, making us feel the warmth of the sun on a summer day). At the same time, each of the materials available for solar cells can only utilize a certain part of this light efficiently. For example, a material which is good for harvesting energy contained in the blue and ultraviolet light will waste energy in the infrared, and vice versa. The elegant solution to this problem is to stack several different materials on top of each other, where each material is chosen to optimally harvest a specific part of the sunlight. However, doing this makes the solar cell much more expensive and tricky to make.

The two factors discussed above combines to the following challenge: a solar cell needs to be fairly technologically advanced to efficiently harvest sunlight, but at the same time it needs to be cheap to manufacture since we need to cover large areas.

Major research efforts are currently ongoing worldwide to find the best solution to this challenge. Researchers are for example looking into new production methods, testing new materials, or developing new ways of structuring or combining already established materials. A significant part of this effort involves the use of various types of nanomaterials.

A nanometer is one billionth of a meter, and nanomaterials are materials which are structured on this length scale. For example, in this thesis we look at a class of materials called nanowires. These are wire-like structures (see Figure 1), where the thickness is between a few and a few hundred nanometers, that means roughly a thousand times thinner than a human hair. Note that the term nanowire refers to the structure of the material, thus "a nanometer-sized wire", not the material itself. We can therefore talk about nanowires made up of different materials, such as gold nanowires, silver nanowires, or silicon nanowires.

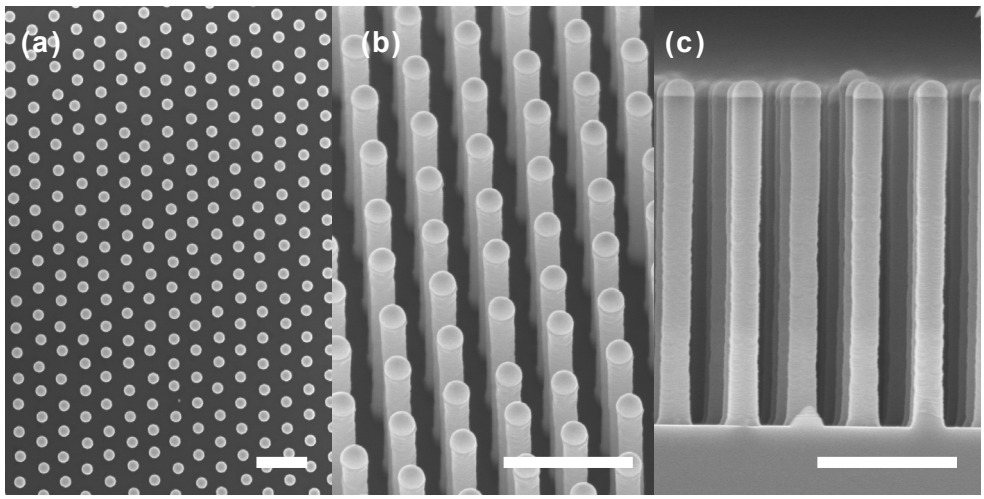


Figure 1: Electron microscope images of a dense "forest" of nanowires, viewed from (**a**) the top, (**b**) an angle, and (**c**) from the side. The nanowires are made on top of a bigger piece of material, called a substrate, visible in c. The white scalebar in each image represents one thousandth of a milimetre.

Recall now how increased solar cell efficiency can be achieved by stacking different materials on top of each other. In addition to making the technology more complex, the materials which are physically best suited to build such a multi-material solar cell are also quite expensive. Best suited are the III-V materials, so named because they are compounds of elements from group III and V in the periodic table. An example is indium-phosphide (InP) containing indium (group III) and phosphorous (group V). Such III-V materials are typically used in solar cells in form of thin layers. In this thesis however, we have looked at the possibility of instead using the III-V material in

nanowire form. The small dimensions of the nanowire gives three potential benefits: First, it can make nanowires absorb light as efficiently as a layer while using less material, due to a different way of interacting with light. Second, it makes it easier to combine different materials stacked on top of each other. And third, it opens up for new and potentially cheaper ways of producing the material. Thus, by making solar cells of III-V nanowires instead of III-V layers, we can possibly manufacture high efficiency solar cells in a cheaper way. However, there is a need to better understand how to make this material, how to control its properties, and the relationship between how the nanowires are made and the solar cell performance. Providing such understanding has been the motivation for this thesis.

When you want to synthesize (make) a nanomaterial, there are two categories of techniques. One is called top-down, where you take a bigger piece of material and controllably remove pieces until you are left with the desired structure, similar to carving a sculpture from a piece of marble. The other is called bottom-up, where you take the building blocks of your structure (for example atoms or molecules) and put them together in the structure you want, similar to building with Lego. The challenge in both of these approaches is that extreme precision is needed, since the structures are so small.

In this thesis we have used a bottom-up approach to synthesize our nanowires, on top of a bigger piece of material (square centimeter sized) called a substrate. The substrate is placed into a reactor chamber where we have good control of conditions such as pressure and temperature. Thereafter the nanowire building blocks (the group III and V elements) are provided via gases we let into the chamber. Interestingly, by carefully tailoring the conditions in the chamber (temperature, gases etc.) and the preparation of the substrate, we can create conditions where the III-V elements spontaneously organize themselves (!) into the nanowire structure. We can design the process to result in dense and ordered "forests" of nanowires (Figure 1) which are good for absorption of sunlight.

In these nanowire forests, we have studied how the synthesis conditions determine how the building blocks combine. For example, by changing the input gases between different stages of the synthesis process, we have studied how to change the electrical properties between different parts of the nanowire. This is important to efficiently extract electricity from the solar cell. Further, we have produced nanowires of different materials which absorb different parts of the sunlight, for use in a multi-material solar cell configuration. It is especially important to have a good electrical connection between such different materials, which we also explored in detail.

Finally, we have produced working nanowire solar cells, where millions of nanowires are contacted in parallel. We have developed a procedure to better characterize how the nanowire solar cell works, and created an improved understanding of how it relates to conditions used during nanowire synthesis and contacting. Our best solar

cell converted energy in the sunlight into electrical energy at an efficiency of 15.0%. This is the best result for a bottom-up synthesized InP nanowire solar cell reported so far. We hope that the work done in this thesis will help increase the efficiency even further in the near future.

Acknowledgements

Sitting down to write this, I feel immensely grateful for the people I have met and all the help and support I have received from so many. To name them all and fully describe what they have all meant to me in this process is not possible in a few pages. Nevertheless, take the following as my humble attempt at expressing my gratitude.

First, I want to thank my main supervisor Magnus. You have always found time to discuss and give input whenever I needed it, and never stopped believing in me. You always impress me with the breadth and the depths of your knowledge, from which I have learnt a lot. I appreciate how you have always taken my opinion seriously, and have given me large freedom in planning and prioritizing my research.

Then, to my co-supervisors. Lars, the way you have combined academic excellence with pioneering entrepreneurship has really created an amazing research environment here in Lund, one it has been a truly rewarding experience to be a part of. Thanks for being an inspiration through your enthusiasm and ideas. Ingvar, thanks for always showing such interest and belief in my project. I appreciate your calm and balanced approach to research; you are always curious, open and hesitant to jump to conclusions. I must also thank you for taking the initiative to let me use the nanoprobe system at Sol Voltaics, which truly was a game-changer in our solar cell research.

To Magnus H, how lucky I was that you were the one who greeted me when I first came to Lund, and patiently and kindly taught me the ins and outs of the lab. I learnt so much from the years we worked together; about imprint, about nanowire growth, about scientific writing, and how to efficiently conduct day-to-day research in the lab. You have always encouraged me and believed in me, also when things were difficult. Thank you also for the lunches and the Malmö-matches!

To Enrique, I am so grateful that you and your family decided to come to Lund. Thanks for everything you have taught me about solar cells, for our endless discussions about the nanoprobe measurements, for the evening runs, the weekend lunches and everything else. Your supportive and positive attitude has been invaluable to me.

To Vilgailė, Xulu, Alexander, Reza, David G, Lukas and Yuwei, for the good collaboration in the group and all the projects we have worked on together. Not everything worked out, but we sure learned a lot!

A significant portion of the work in this thesis has been done in collaboration with people from Sol Voltaics. I am indebted to Christian, for all your work with

processing of the solar cells, and for teaching me the Kleindiek system. It has been great to work with someone as thorough, friendly and helpful as you. Thanks to Erik for our discussions about the nanoprobe measurements, and for sharing all your helpful tips about how to conduct the measurements efficiently. Damir, thanks for your help with processing and for digging up old data. To David, Polly, Shishir, James, Linda, Yuxuan, Giuliano and all the rest for always being helpful and welcoming.

Another big chunk of this thesis deals with doping characterization. In these projects, it has been great to work with people as skilled and knowledgeable as Olof, Renato, Ali, Fredrik, Kristian and Tuomas. Thanks for the good collaborations, and for doing such interesting measurements on my nanowires!

To Nicklas, Yang and Pyry, for me as an experimentalist to have the opportunity to discuss solar cell physics with people who have such a deep theoretical understanding and overview has been a true privilege. Maybe one day we can make cells as good as the ones you model.

To Laura, my office mate, thanks for sharing all the laughs and all the venting of frustration. Thanks for feeding me with candy and for opening the window when I have consumed all the oxygen without noticing.

Thanks to Sebastian, for always being willing to help with and discuss growth related issues.

Thanks to all past and present fellow PhD-students and researchers at FTF. So many interesting and talented people, it has been a pleasure to work with you all over the years.

Thanks to all the collaborators in the European Nano-Tandem project. Our meetings have always been interesting and rewarding.

To Jesper, Lert and Andrea, for the collaborations on the synchrotron experiments.

Thanks to Heiner, Dan, Anneli and Anders for leading and developing the division and NanoLund in such an excellent way.

Thanks to Ivan, Maria, Mariusz, Håkan, Sara, George, Anders, Peter, David, Dmitry, Sören and Bengt, for all your help and your hard work keeping Lund Nano Lab in shipshape. A special thanks to Mariusz for all the help with nanoimprint-related things, and to Peter for your tireless work with keeping the Aixtron running.

Thanks to Abdul-Rehman, Charlotte, Mia, Margareta, Monica, Louise, Mari, Gerda, Line, Johanna and Janne for always helping out with practical, administrative and IT-related things.

I want to thank my friends living near and far, which I don't see nearly as often as I would like to. A special thanks to Heine, Thomas, Trude and Mari, for all the fun

weekend and holiday visits. I am grateful that we have managed to spend so much time together despite the distance, and I look forward to living closer to you all.

Thanks to Lise, Rolf Arne, Kristin and all the others in Horten, it's always nice to come visit!

To my brothers, Sondre and Bendik, you never cease to inspire me, challenge me and make me laugh, each in your own way. To Unn-Iren, Monja and Selma, you make Hamre an even richer and happier place to come home to.

To my parents, you have always encouraged me to follow my interests and develop my talents, no matter how far from home it has taken me. I am forever grateful for your love and support, and for giving me a solid foundation of values to guide me in times of doubt and difficulty.

And finally, if I have learnt a lot about science and research during these years, that's nothing compared to what I have learnt about myself. Camilla, I couldn't have done it without you by my side. I am so grateful to have met you, that you moved to Sweden to be with me, and that we will now start the next chapter in our lives together. I love you.

Gaute Otnes
Lund, January 2018

List of Papers

This thesis is based on the following papers, which will be referred to by their roman numerals in the text.

I. **Towards high efficiency nanowire solar cells**
G. Otnes and M. T. Borgström
Nano Today, 2017, 12, 31-45
I performed the literature search, organized the information and wrote the paper

II. **Strategies to obtain pattern fidelity in nanowire growth from large-area surfaces patterned using nanoimprint lithography**
G. Otnes, M. Heurlin, M. Graczyk, J. Wallentin, D. Jacobsson, A. Berg, I. Maximov and M. T. Borgström
Nano Research, 2016, 9, 2852-2861
I performed a majority of the nanoimprint lithography (NIL) and nanowire growth experiments. I did the photoluminescence measurements. I was responsible for analyzing the data and for writing the paper.

III. **Comparing Hall Effect and Field Effect Measurements on the Same Single Nanowire**
O. Hultin, G. Otnes, M. T. Borgström, M. Björk, L. Samuelson and K. Storm
Nano Letters, 2016, 16, 205-211
I performed NIL and developed the nanowire growth. I participated in discussions regarding the results and wrote the part of the paper relating to nanowire growth.

IV. **Simplifying Nanowire Hall Effect Characterization by Using a Three-Probe Device Design**
O. Hultin, G. Otnes, L. Samuelson and K. Storm
Nano Letters, 2017, 17, 1121-1126
I performed NIL and developed the nanowire growth. I participated in discussions regarding the results and writing of the paper.

V. **$In_xGa_{1-x}P$ Nanowire Growth Dynamics Strongly Affected by Doping Using Diethylzinc**
G. Otnes, M. Heurlin, X. Zeng and M. T. Borgström
Nano Letters, 2017, 17, 702-707
I performed NIL and the nanowire growth experiments. I analyzed the data and was responsible for writing the paper.

VI. **Electrical and optical evaluation of n-type doping in $In_xGa_{1-x}P$ nanowires**
X. Zeng*, R. T. Mourão*, G. Otnes*, O. Hultin, V. Dagytė, M. Heurlin and M. T. Borgström
*These authors contributed equally
Submitted
I performed NIL and developed the nanowire growth. I wrote parts of the paper and participated in discussions regarding the results.

VII. **InP/GaInP nanowire tunnel diodes**
X. Zeng, G. Otnes, M. Heurlin, R. T. Mourão and M. T. Borgström
Nano Research, 2017, doi: 10.1007/s12274-017-1877-8
I performed the electron beam induced current characterization, and wrote the part of the paper relating to these measurements. I participated in discussions regarding the results.

VIII. **Understanding InP Nanowire Array Solar Cell Performance by Nanoprobe-Enabled Single Nanowire Measurements**
G. Otnes, E. Barrigón, C. Sundvall, E. Svensson, M. Heurlin, G. Siefer, L. Samuelson, I. Åberg and M. T. Borgström
Submitted
I performed NIL, developed the nanowire growth and performed the single nanowire measurements. I analyzed the data and wrote the paper.

Papers not included

The following papers are not included since they are beyond the scope of this thesis. They are listed in chronological order

IX. **Doping evaluation of InP nanowires for tandem junction solar cells**
F. Lindelöw, M. Heurlin, G. Otnes, V. Dagyte̊, D. Lindgren, O. Hultin, K. Storm, L. Samuelson, M. T. Borgström
Nanotechnology, 2016, 27, 065706

X. **InP nanowire p-type doping via zinc indiffusion**
T. Haggren, G. Otnes, R. Mouraõ V. Dagyte̊, O. Hultin, F. Lindelöw, M. T. Borgström and L. Samuelson
Journal of Crystal Growth, 2016, 451, 18-26

XI. **Absorption and transmission of light in III-V nanowire arrays for tandem solar cell applications**
N. Anttu, V. Dagyte̊, X. Zeng, G. Otnes, and M. T. Borgström
Nanotechnology, 2017, 28, 205203

XII. **Time-resolved photoluminescence characterization of GaAs nanowire arrays on native substrate**
V. Dagyte̊, E. Barrigón, W. Zhang, X. Zeng, M. Heurlin, G. Otnes, N. Anttu and M. T. Borgström
Nanotechnology, 2017, 28, 505706

XIII. **GaAsP Nanowire Solar Cell Development Towards Nanowire/Si Tandem Applications**
E. Barrigón, Y. Chen, G. Otnes, V. Dagyte̊, N. Anttu, L. Samuelson and M. T. Borgström
Proceedings of the 44th IEEE Photovoltaic Specialists Conference , 2017

XIV. **Growth and optimization of GaInP/InP nanowire tunnel diode**
X. Zeng, G. Otnes, M. Heurlin and M. T. Borgström
Proceedings of the 44th IEEE Photovoltaic Specialists Conference , 2017

1 Introduction

The economic growth and increased prosperity since the industrial revolution has been crucially dependent on the access to cheap energy through burning of fossil fuels. Over the last decades however, there has been increasing concern that our fossil-based energy system, and the resulting emission of greenhouse gases, is not sustainable. Most importantly, the Intergovernmental Panel on Climate Change (IPCC) concludes in their latest report that anthropogenic greenhouse gas emissions are *"extremely likely"* to have been the dominant cause of the observed climate warming during the last 70 years [1]. IPCC further states that a continuation of our high emissions will continue to warm the climate, and *"lead to mostly negative impacts for biodiversity, ecosystem services and economic development and amplify risks for livelihoods and for food and human security"* [1]. The risk of such negative impact is magnified as the warming increases. To keep the warming at what is hoped to be a manageable level, the United Nations have agreed to limit the increase in global average temperature to 2 ^{0}C compared to pre-industrial levels. To have a likely chance of staying within the 2 ^{0}C-target, IPCC predicts that a reduction in greenhouse gas emissions of 40-70% is needed by 2050, relative to 2010 levels [1]. Reducing emissions at this scale will demand a transition to a low-emission energy system. This constitutes an enormous challenge, especially as it needs to happen while at the same time providing enough energy for a growing world population [2], in which more than 700 million people should be lifted out of poverty [3].

A wide range of combined efforts are needed to transition into a sustainable energy system, requiring major investments in a number of low-emission technologies [4]. A technology that will need to play an important role is solar photovoltaic (PV) devices, commonly referred to as solar cells, converting sunlight directly into electricity. Energy in the form of sunlight is abundant, but historically high cost has prevented solar PV from competing with fossil based alternatives on a large scale. However, prices have been declining steadily as the market has grown (Figure 1.1a), tracking a learning curve where every doubling of the production capacity is accompanied by a ~20-25% solar module price cut [5, 6]. As production capacity has grown annually at an average of 40% since the beginning of the century [5, 7], this has led to a rapid price drop. The last part of the price and production capacity development is illustrated in Figure 1.1b, for the period between 2008 and 2016. As the cost has decreased, solar PV has become increasingly competitive in different energy markets

[6]. To continue this trend[1], and make solar PV the large supplier of clean energy it needs to be, further price reductions are required.

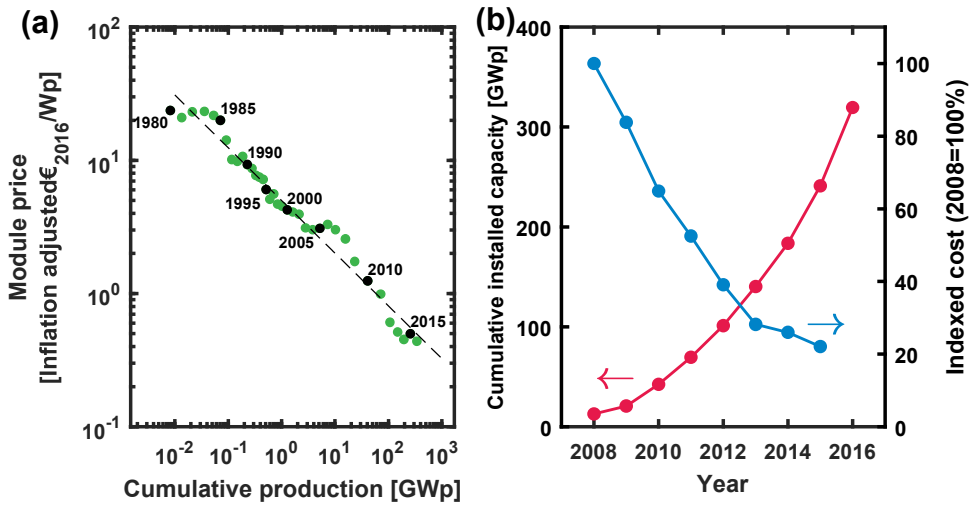


Figure 1.1 Historic price and global capacity development for photovoltaic technology. (**a**) Module prices as a function of cumulative production capacity. The dashed line represents a 24% learning curve. Data from ref. [7]. (**b**) Development of the cumulative production capacity (red, left y-axis) and cost of utility scale PV (blue, right y-axis) in the period 2008-2016. Data from ref. [7, 8]

To bring down the price of electricity produced by a PV module one can, simply put, either make the module cheaper or more efficient (while keeping the other variable constant). However, looking at a full utility-scale solar PV system, the cost of the PV module itself now constitutes less than 50% of the total cost [9, 10]. This share has become smaller as the cost of the module has decreased faster than for other parts of the PV system, such as costs related to inverters, wiring, land use, financing, labour and so on [9]. Therefore, improving the module efficiency has become increasingly important from an economic perspective, as a higher efficiency module will cut all parts of the total cost scaling with system size [9–11].

Today, 94% of all solar PV systems sold are based on single junction Si solar cells [5]. However, the efficiencies of Si solar cells have improved quite slowly over the last couple of decades, recently with an annual absolute efficiency improvement of 0.04-0.09% [10]. Further, the current lab cell efficiency record of 26.7% [12] is getting

[1] Note that for solar energy (and most other renewable energy technologies) to penetrate the energy market on a large scale, significant development in energy storage solutions are needed. Interesting discussions of development in this field can be found e.g. in ref. [142].

close to what is considered practical efficiency limits for the Si single junction technology [11, 13]. Therefore, a major research effort is targeted at finding alternative solar cell technologies, capable of achieving higher efficiencies [14]. Especially interesting are those which can be added on to conventional Si cells to boost their performance, while leveraging existing industrial infrastructure [11]. An interesting research direction in this regard is the use of various nanostructured materials [15, 16]. In this thesis, we study one of the materials that have received increasing attention in recent years, namely semiconductor nanowires.

Nanowires are elongated structures with diameters ranging from a few to a few hundred nanometers, and lengths typically in the 1-10 μm range, depending on the application. Semiconductors in the nanowire geometry have been an area of intense research over the last couple of decades, with potential applications in a wide range of areas, including e.g. electronics, photonics, thermoelectrics, cell biology, battery technology, as well as PV [17]. We note that a PV device is any device converting light to electricity through the photovoltaic effect, in principle also including e.g. optical sensors and PV micro power generators. For a PV device to be a solar cell however, an additional requirement is that it covers a reasonably large area, making practical amounts of solar power generation possible. In this thesis we will focus on and use the term *nanowire solar cell* to describe devices made of arrays of vertical nanowires. Such arrays have the potential to be upscaled and used to harvest significant amounts of solar energy.

Semiconductor nanowires were first used for PV in hybrid organic-inorganic (2002) [18] and dye-sensitized (2005) [19–21] architectures. The first single nanowire PV devices containing a *pn*-junction were realized in Si (2007) [22, 23] and GaAs (2008) [24, 25]. Shortly thereafter (2009), a larger area device consisting of an array of vertical bottom-up synthesized *pn*-junction III-V nanowires was presented, having a power conversion efficiency of 3.4% [26]. The power conversion efficiency of such nanowire solar cells has since then increased substantially, with the current world record of 15.3% held by a GaAs device (2016) [27]. Recently, a top-down synthesized InP nanowire solar cell reached an efficiency of 17.8% [28]. This thesis studies the synthesis and characterization of nanowire solar cells, with the experimental work focused on bottom-up synthesized nanowire arrays in the InP/$In_xGa_{1-x}P$ materials system.

1.1 Thesis outline

To understand how we can achieve improvements in a solar cell technology, we need an understanding of the workings and limitations of current devices. Providing this is the aim of Chapter 2, starting with an introduction of some basic solar cell theory.

Thereafter the potential benefits offered by the nanowire geometry are discussed. The chapter ends with a description of some design guidelines followed when synthesizing the nanowires studied in this thesis. These guidelines are based on the current understanding of what is needed to achieve good nanowire solar cell performance.

Even though significant knowledge exists regarding the specific characteristics a high performing nanowire solar cell should have, synthesizing such a device is still a challenge. To understand where the challenging aspects lie, an understanding of the synthesis techniques is required. An introduction to the synthesis techniques used in this thesis is given in Chapter 3. The chapter ends with a discussion of specific challenges in synthesizing high quality nanowire arrays, discussed in relation to the different papers included in this thesis.

To understand the connection between synthesis conditions, material properties, and device performance, a variety of characterization techniques are needed. In Chapter 4, we discuss the techniques used in this thesis to characterize nanowire morphology, doping, electrical characteristics and solar cell performance.

In Chapter 5, the thesis work is summarized, ending with a discussion on some interesting challenges and opportunities ahead for nanowire solar cell technology.

2 Nanowire solar cells

A comprehensive discussion of nanowire solar cells is given in Paper I, where the research literature on the topic as of August 2016 is reviewed, mainly focused on III-V materials. In this chapter, we will first provide some background on solar cell basics not given in Paper I. Thereafter, we will discuss benefits the nanowire geometry holds as a solar cell material, before ending with a brief discussion on how a nanowire solar cell should be designed. Through this discussion the context and motivation of the studies in this thesis will be given. A rigorous or full treatment of fundamental physics and design considerations for solar cells is not the objective of this text, but rather to lay the foundation for later discussions relating to nanowire solar cell synthesis and performance.

2.1 Solar cell basics

In a solar cell, energy in the form of light from the Sun is transformed into electrical energy, proceeding in two fundamental steps: First, the photons in the sunlight are absorbed in the cell by transferring their energy to the charge carriers in the cell material, and second, these charge carriers are separated and extracted through an external circuit. Typically, the active part of the solar cell is made of an inorganic semiconductor *pn*-junction[2], where both of these steps take place.

In a semiconductor, absorption of sunlight happens by the excitation of electrons across the bandgap, creating a free electron in the conduction band and a free hole in the valence band. Between the electron and the hole, an energy difference now exists. This energy difference will eventually dissipate as the carriers recombine. Before this happens spontaneously in the material, the task of the solar cell is to separate the two charge carriers and force them to instead recombine through an external circuit, where the energy difference can be put to use. This task is solved by the electric field of the *pn*-junction, leading holes to drift towards the *p*-side and electrons towards the *n*-side (Figure 2.1), resulting in a photocurrent, I_{ph}. Ideally, this photocurrent can be

[2] Solar cells not based on inorganic semiconductor *pn*-junctions, such as dye-sensitized or organic solar cells, also constitute an active research area, but will not be discussed further here.

added to the current *(I)* –voltage *(V)* characteristics of the *pn*-junction in the dark (Figure 2.2), according to the so-called superposition principle. The dark *IV* characteristics are given by the diode equation,

$$J(V)_{dark} = J_0\left(e^{\frac{eV}{nkT}} - 1\right) \qquad \textbf{2.1}$$

Where J_0 is the saturation current density, e is the elementary charge, n is the ideality factor, k is the Boltzmann constant, and T is the temperature. Note that we have switched from currents to current densities here, to make our discussion independent of the exact geometry of the device. We will stick to the use of current densities for the rest of this thesis.

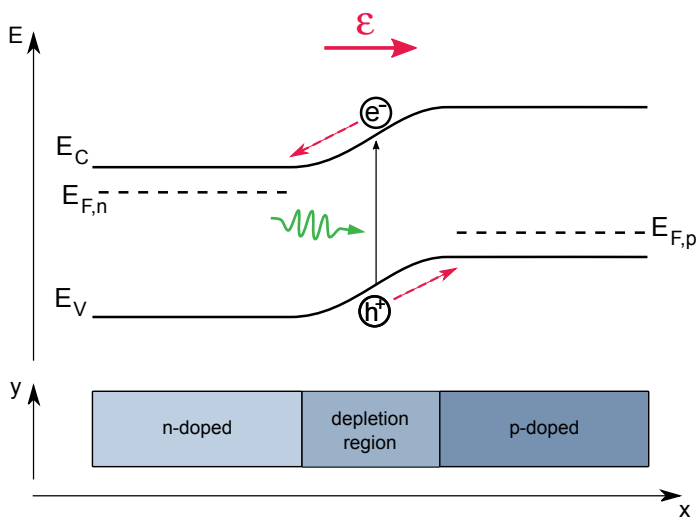


Figure 2.1 Schematic illustration of a *pn*-junction, consisting of a *p*- and an *n*-doped segment, creating a depletion region between them. After excitation of an electron-hole pair by a photon, the built-in electric field in the depletion region, ε, sweeps the electron to the *n*-side and the hole to the *p*-side, resulting in a photocurrent.

By use of the superposition principle we add the photocurrent to Equation 2.1 and get

$$J(V)_{light} = J_0\left(e^{\frac{eV}{nkT}} - 1\right) - J_{ph} \qquad \textbf{2.2}$$

To extract electrical energy from our solar cell, it needs to be connected in series with an external load. Let us first consider the two extreme cases of such a load, having zero or infinite resistance. When the resistance is zero, the *p* and *n* sides of the solar

cell are short-circuited, V=0 and Equation 2.2 gives the short circuit current density, J_{SC}, as

$$J_{SC} = J_{ph} \qquad \textbf{2.3}$$

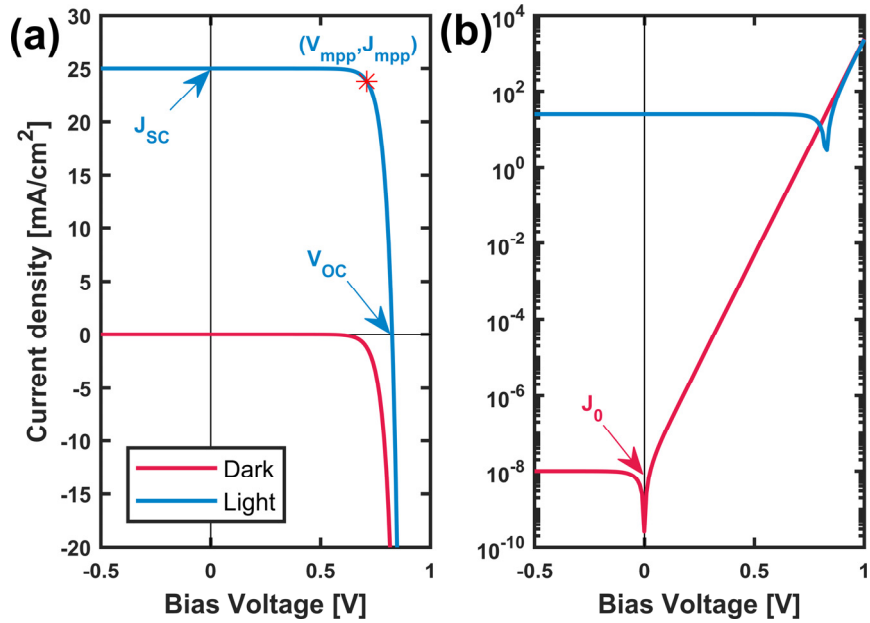


Figure 2.2 Plot of example diode *IV* characteristics in the dark (red line) and under illumination (blue line), with (**a**) linear and (**b**) logarithmic *y*-axis.The plot was made for a diode having $J_0 = 1 \times 10^{-8}$ mA/cm^2, n= 1.5 and producing a photocurrent of 25 mA/cm^2. Key light and dark *IV* parameters have been indicated in (a) and (b), respectively.

The other extreme case of an infinite resistance yields J=0, we have an open-circuit, and Equation 2.2 and 2.3 gives (noting that $e^{eV/nkT}$>>1 for relevant V-values) the open circuit voltage, V_{OC}, as

$$V_{OC} = \frac{nkT}{eV}\ln\left(\frac{J_{SC}}{J_0}\right) \qquad \textbf{2.4}$$

Electrical power output of the solar cell will be maximized by choosing the external load such that the product of the current and the voltage is maximized. Obviously, this does not happen at neither zero nor infinite resistance of the external load, but somewhere in between these two extremes, at what is referred to as the maximum power point. Here, the current density and voltage is denoted as J_{mpp} and V_{mpp}.

Comparing this output power, P_{out}, to the input power, P_{in} (total power of the light incident on the cell), we can define a power conversion efficiency, *PCE*,

$$PCE = \frac{P_{out}}{P_{in}} = \frac{J_{mpp} \times V_{mpp}}{P_{in}} = \frac{J_{SC} \times V_{OC} \times FF}{P_{in}} \quad \textbf{2.5}$$

In the last step of Equation 2.5, a parameter called the fill-factor, *FF*, is introduced. It is defined as the ratio between the products $J_{mpp} \times V_{mpp}$ and $J_{SC} \times V_{OC}$ and is a measure of the "squareness" of the *IV*-curve (Figure 2.2a).

Several losses contribute to the *PCE* of a real solar cell being less than 100 %. We will in the following discuss these losses grouped either as fundamental or non-fundamental losses. In simple terms, the fundamental losses set limits to the performance of an ideal device of a given design, while the non-fundamental losses depend on factors constituting deviations from this ideal performance.

2.1.1 Fundamental losses

To understand the fundamental losses, we first need to consider the source of input energy to our solar cell, namely the incoming sunlight. The light emitted from the Sun can be modelled quite well by blackbody radiation corresponding to its surface temperature of about 5760 K [29] (Figure 2.3). Going through the atmosphere of the Earth, some parts of the spectrum will be significantly attenuated by scattering and/or absorption. Accounting for this attenuation, the standard reference spectrum to describe the spectral distribution of light reaching the surface of the Earth is the AM1.5G-spectrum[3], also plotted in Figure 2.3.

[3] The magnitude of scattered/absorbed light intensity will vary (disregarding cloud cover) dependent on the distance of the atmosphere traversed by the light. This distance is dependent on the angle of the sun relative to zenith, θ, and thus on the longitude, time of day and time of year. The Air Mass (AM) number (=1/cos(θ)) is typically used to denote different spectra, where e.g. AM0 is the spectra outside the Earth's atmosphere, and AM2 is the spectrum at θ=60 ^{0}. As a standard to compare different solar cell technologies, the AM1.5G is typically used, normalized to 1 kW/m^2. The G denotes a global spectrum, including also diffuse light, in contrast to the spectrum containing only the direct component, AM1.5D.

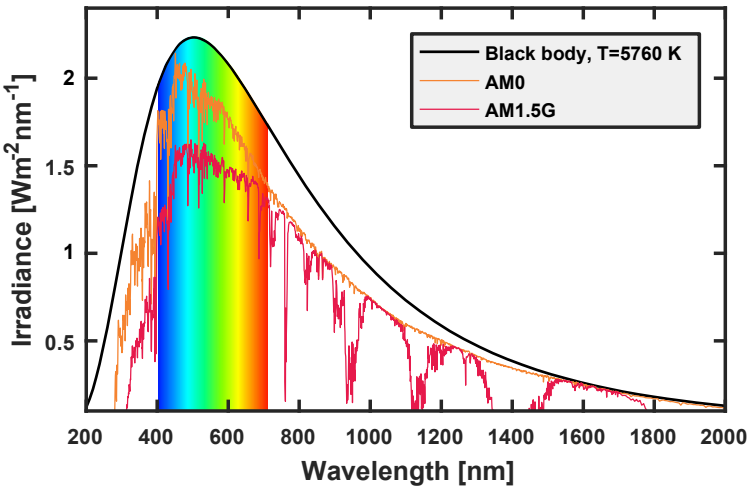


Figure 2.3 The solar spectrum. A blackbody spectrum corresponding to the Sun's surface temperature, plotted together with the spectrum outside the Earth's atmosphere (AM0) and the spectrum reaching the surface of the Earth (AM1.5G). The rainbow colors indicate the wavelength region visible to the human eye. Spectra taken from ref. [30].

A key point to note from the solar spectrum in Figure 2.3 is how the solar energy is distributed between photons of a range of different energies, from the ultraviolet (UV) part of the spectrum and well into the infrared (IR). Therefore, it is important to consider how light of different energies interact with the solar cell. In Figure 2.4, an illustration is given of the fate of two photons of different energies as they move through the semiconductor. Photons with energy higher than the bandgap will be absorbed (Figure 2.4, left), but any energy in excess of the bandgap will be rapidly lost to thermalization, i.e. lost to heat as the charge carriers thermalize to the band-edges via phonon emission[4]. On the other hand, photons with energy lower than the bandgap will simply not be absorbed (Figure 2.4, right). The magnitudes of these losses have opposite dependencies on the size of the bandgap, i.e. lowering the bandgap of the cell will lead to less absorption losses but increase thermalization losses, and vice versa. Hence, we can understand that an optimal bandgap exists for maximized *PCE*. This can be calculated in the detailed balance approach, first done by Shockley and Queisser in 1961 [31], where an optimum of ~31%[5] is found for a

[4] In hot-carrier solar cell concepts, the key strategy to increase *PCE* is to extract the charge carriers prior to the thermalization process, through energy selective contacts. A working hot-carrier solar cell has recently been realized in a single nanowire [143].

[5] Values of efficiency limits/losses in this chapter are provided to give a feeling for their magnitude, and are given only as approximate values. This since they vary somewhat (a few percentage points) between different reports, due to variations in assumptions and methods (e.g. the spectrum used) in the calculations.

single bandgap of ~1.3 eV. This efficiency is usually referred to as the Shockley-Queisser limit, named after the authors of the original study. Note that different detailed balance/Shockley-Queisser limits can be calculated also for other cell concepts/light conditions (discussed further below), but we will in this thesis use the Shockley-Queisser term to refer only to the limit calculated for a single junction solar cell under 1-sun light conditions. Experimentally, the best single-junction solar cells are slowly improving towards the Shockley-Queisser limit, with the current record held by a GaAs cell of 28.8% [32].

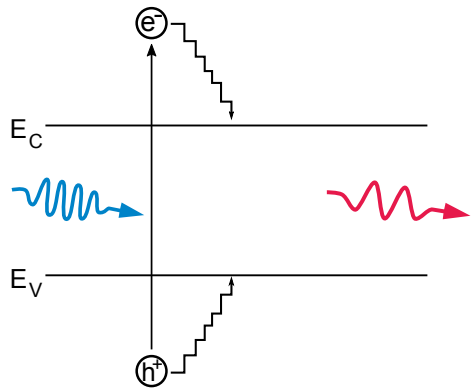


Figure 2.4 Schematic illustrating the fate of a photon with energy much higher than the bandgap (blue) and a photon with energy less than the bandgap (red), as they move through a semiconductor. The high energy photon will have a high probability of being absorbed, but the excited carriers will quickly loose a major part of the photon energy as they relax to the band edges. All the energy of the low energy photon will be lost as it cannot be absorbed in the semiconductor.

A number of different cell designs are being actively studied in which thermalization and absorption losses can be reduced compared to the single junction design, these designs are thus able to reach efficiencies beyond the Shockley-Queisser limit [14]. These include exploratory concepts such as hot-carrier solar cells [33], upconverter/downconverter strategies [34], intermediate band solar cells [35], and multi-exciton generation concepts [36]. However, the only design so far to experimentally deliver efficiencies beyond the Shockley-Queisser limit is the multijunction solar cell, consisting of a number of different sub-cells with bandgaps chosen to absorb different parts of the solar spectrum. Even though approaches where the spectrum is spatially distributed onto different sub-cells by external optics are possible, the most common design is one where the different sub-cells are stacked on top of each other (Figure 2.5) [37]. The sub-cells should be stacked with the highest bandgap on top, and then with progressively smaller bandgap moving down the stack, allowing each cell to absorb photons with above bandgap energy while transmitting remaining photons to be absorbed in the underlying cells. Thus, the sub-cells

distribute the spectrum between themselves with no external optics. By going from a single junction to a double-junction cell, the efficiency limit increases from ~31 to ~43%, while an infinite stack of subcells has a limit of ~68% [38]. Experimentally, the current world record for any solar cell technology at 1-sun intensity is held by a multijunction solar cell consisting of 5 sub-cells, with an efficiency of 38.8% under the AM1.5G spectrum [32].

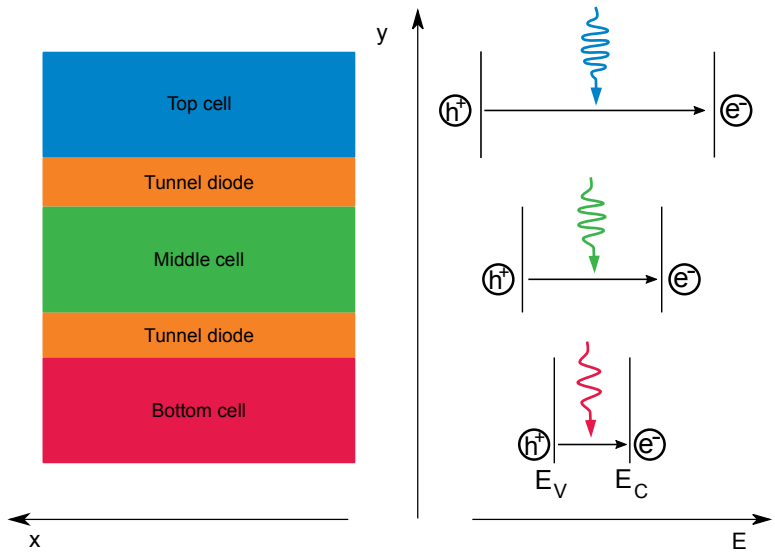


Figure 2.5 Schematic of a triple-junction solar cell. The three subcells of different materials are stacked on top of each other, with bandgap energy decreasing from top to bottom. In this way, the different energy photons in the solar spectrum are distributed between the different cells to make optimal use of their energy. The different subcells are connected in series by tunnel diodes. In a real multijunction cell, a number of additional layers are typically present, but are omitted here for simplicity.

In addition to the thermalization and absorption losses, some other mechanisms also need to be considered when calculating the efficiency limits for a given design. Understanding the details of these losses is beyond the scope of this thesis, and the interested reader can find thorough treatments of these topics e.g. in references [39–41]. However, one of the losses is relevant to later discussions, and a brief introduction is appropriate here. The loss stems from the fact that while absorbed light in the cell is incident at a very narrow angle[6], light emitted from the cell (Kirchoff's law states that absorbers must also be emitters) is omnidirectional. This

[6] The Sun emits light isotropically in all directions, but due to the distance between the Sun and the Earth only a small portion of this light hits the Earth, thus the light is incoming at a very small solid angle. For most practical purposes, the light can be considered a parallel stream of photons.

mismatch results in an entropy increase, constituting an energy loss which lowers the efficiency of the cell. Reducing this loss is possible by making the emission and absorption angles more equal to one another. Conventionally, this has been done through use of concentrating optics to focus the incoming light onto a small cell area, increasing the absorption angle of the cell. This increases the efficiency limit for an infinite number of subcells in a multijunction approach from ~68% for no concentration to ~85% for full concentration[7] [39, 40]. The current world record for concentrated light is held by a four-junction cell at 46% efficiency under the AM1.5D spectrum [32]. Equivalently to increasing the absorption angle, one could instead restrain the emission angles of the device [39]. This can be done by simply putting a back-reflector on the cell [42], or additionally by more advanced photonic design principles to guide light emission only in certain directions [43]. The nanowire geometry might offer some benefits in this regard, as will be discussed further in Chapter 2.2.

2.1.2 Non-fundamental losses

In real solar cells, the *PCE* fall short of fundamental limits for a given design due to a number of imperfections. In the following we will discuss these imperfections and their effect on the three key *PCE* parameters (Eq. 2.5); J_{SC}, V_{OC}, and *FF*.

Optical losses

When calculating the efficiency limits, it is typically assumed that all incoming light with energy higher than the bandgap is absorbed. In a real device, this is not the case for two reasons. First, a portion of the light will not even enter the semiconductor, due to reflectance at the air-semiconductor interface, shading losses of the metal contact grid, or by parasitic absorption in supporting layers (such as transparent conductive oxides). Reflectance losses are typically minimized by use of antireflection (AR) coatings and/or surface texturing, while losses due to contact grid and supporting layers are tackled by optimizing design and/or materials properties. Second, since the solar cell has a finite thickness, some light will travel through the structure without being absorbed. This is of special concern since the cell should be kept reasonably thin, due to material cost and other reasons which will become apparent in a while. Therefore, scattering features at surfaces and interfaces are sometimes incorporated to scatter the light into the cell in non-orthogonal directions, thereby increasing the optical path length in the material. Higher than bandgap energy light which is not absorbed in the solar cell leads to a sub-optimal J_{SC}.

[7] The theoretical maximum concentration corresponds to a concentration factor of ~46000, for derivation see ref. [42]

Recombination losses

Efficiency limits are typically calculated in the radiative limit, meaning that carrier recombination in the device takes place solely through radiative recombination. In a real device however, a substantial fraction of the recombination will typically be non-radiative. The non-radiative recombination is frequently classified according to the regions of the cell where it takes place (contact, surface, quasi-neutral or depletion region, bulk or perimeter), and/or its mechanism (Auger, Shockley-Read-Hall). Non-radiative recombination can affect both J_{SC} and V_{OC} in the device.

The J_{SC} will be lowered if the recombination is high enough to prevent photogenerated minority carriers from diffusing to the charge separating junction and contribute to the photocurrent. In materials exhibiting short bulk diffusion lengths, such as amorphous silicon, a long intrinsic segment is typically added to make the *p-n* junction into a *p-i-n* junction [29]. The depletion region now stretches throughout the intrinsic segment, where the built-in electric field enhances charge carrier collection instead of relying on diffusion [44].

The V_{OC} is the voltage at which the total current through the solar cell is zero, thus the photogenerated current is perfectly balanced by an opposite current in the forward biased diode. From the diode equation (Equation 2.1), we see that the current in the forward biased diode depends on its saturation current J_0, which is a common measure of the recombination in the device. A higher recombination will give a higher J_0, and hence a balancing current for the photocurrent ($J(V)_{light} = 0$ in Eq. 2.2) is achieved at lower voltages. In other words, minimizing J_0 is reflecting a lowering of recombination in the solar cell, which is essential in achieving a high V_{OC} (as expressed in Eq. 2.4). However, J_0 is a fairly complicated parameter to understand and optimize. Most importantly, while basic models typically treat J_0 as a constant, it actually varies depending on the excess carrier concentration, and hence the voltage bias and/or the illumination intensity [45]. Further, recombination is different in various parts of a device, hence different local J_0 values can in principle be assigned to each part. Thus, we need to understand which J_0-value is of relevance to us, and how to find it. As a first approximation, J_0 -values for a given solar cell are typically extracted by fitting the forward bias dark *IV* characteristics to the diode equation (Equation 2.1). Here, J_0 will vary depending on the bias region where the fit is made, but the most relevant J_0 is the one extracted at biases close to the expected V_{OC}. Note that this value is a global J_0, lumping recombination characteristics for the entire device into one parameter. Using the dark *IV* curve to extract J_0 relies on the approximation that the recombination does not change significantly when photogenerated excess carriers are introduced. While this holds in many situations, it might not always be a valid approximation, as discussed for InP nanowire solar cells in Paper VIII.

To enable fits to experimental data, the diode equation typically contains an ideality factor, n (as in Eq. 2.1). Similar to J_0, the value of n might differ both between devices and for the same device depending on e.g. voltage bias. The value of n typically lies between 1 and 2, and gives a clue as to which recombination mechanism and/or region of the device is dominant. For example, while both radiative recombination in the whole device and Shockley-Read-Hall recombination in the quasi-neutral regions give an ideality factor of 1, Shockley-Read-Hall recombination in the depletion region gives an ideality factor of 2. Note that the basic diode equation is often expanded to contain more than one diode, with different n and J_0 values, if needed to better explain the experimental data.

In general, recombination is reduced by improving the material quality and optimizing the doping profiles. Recombination sites of special concern are the surfaces and interfaces in the cell, as they are unavoidable. Two steps are typically taken to minimize recombination at surfaces and interfaces. First, surfaces are passivated by adding a layer which reduces the surface recombination, e.g. by saturating dangling bonds. Second, an adjacent layer to the surface/interface can be designed as a barrier for minority carriers to reach the surface/interface. This is typically done by introducing high doping in the adjacent layer, often combined with a heterostructure providing an appropriate band-offset. Recombination at surfaces is of special concern in nanowire solar cells due to their large surface to volume ratio, as discussed in Paper I and Paper VIII.

Resistive losses

While the efficiency limit calculations typically neglect resistance effects in the solar cell, these can have significant impact on the *PCE* in real devices. The relevant resistance effects are typically modelled in terms of a series resistance, R_S, and a shunt resistance, R_{SH}, as shown in the equivalent circuit diagram in Figure 2.6.

The contributors to R_S are the resistance of the semiconductor material along the current path, the contact resistance between the semiconductor and the metal/ITO, as well as the resistance within the contact material. The value of R_S should be as low as possible, since a high R_S will lower the *FF*, and even the J_{SC} at high values (Figure 2.6b).

The contributors reducing R_{SH} are all leakage paths around the *pn*-junction. The possible sources of such leakage paths are numerous and varied in character, e.g. as discussed for Si solar cells in ref. [46]. The value of R_{SH} should be as high as possible, since a low R_{SH} will lower the *FF*, and even the V_{OC} at low values (Figure 2.6c).

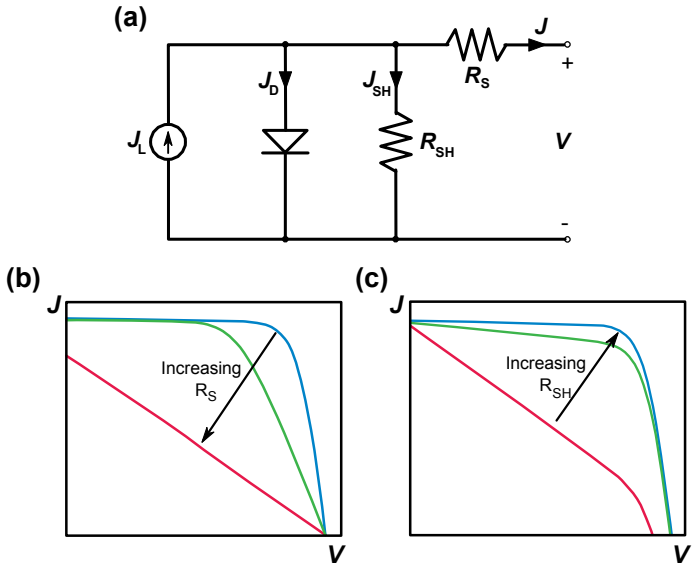


Figure 2.6 Parasitic resistances. (**a**) Typical equivalent circuit diagram of a solar cell, with the parasitic resistances modelled as a shunt resistance, R_{SH}, in parallel with the diode, and a series resistance, R_S, in series with the diode. (**b**) *IV*-curve showing the effect of different values of R_S on the solar cell performance. (**c**) *IV*-curve showing the effect of different values of R_{SH} on the solar cell performance

2.2 Benefits of the nanowire geometry

With the basic solar cell physics now established, we will continue our discussion by addressing the following question: Why would one want to use III-V semiconductors in the form of nanowires as a solar cell material? The answer to this question starts with looking at the competitiveness of thin-film III-V solar cells.

For a solar cell technology to be competitive, it should ideally achieve high efficiency while maintaining low cost[8]. The III-V materials have excellent properties for solar cells, and have a number of compounds available with bandgaps relevant to make multijunction solar cells (Chapter 2.1.1). Consequently, the III-V materials hold efficiency records for any number of junctions [32]. However, they have so far not been competitive for terrestrial applications, due to their high manufacturing cost. In

[8] Some solar cell concepts, such as organic solar cells, might due to very low cost prove competitive despite fairly low efficiencies, in certain markets. However, due to system costs other than the solar cell itself, obtaining high efficiencies is increasingly important to compete on a large scale, as discussed in Chapter 1.

this regard, moving from thin-films to the nanowire geometry in this material system holds several potential benefits, as discussed in the following.

First, by utilizing geometry dependent absorption resonances in the nanowires, strong absorption is possible using only small volumes of the expensive III-V materials [47]. As an example, comparing the InP nanowire solar cell reported in Paper VIII to the best planar InP cell [48], the J_{SC} for the nanowire cell is 86% of the planar value, while the volume of active III-V material is only 6%.

Second, the nanowire geometry offers relaxed lattice matching requirements during epitaxial growth. This arises from the small nanowire footprint, where strain due to lattice mismatch can relax radially via the free surface [49]. The relaxed lattice matching requirements open up for growth on foreign substrates (as discussed further in Chapter 3.3), potentially much cheaper than the substrates used for growth of conventional planar III-V solar cells. The substrate could also potentially be reused after removing the nanowires from the substrate embedded in a polymer that can be delaminated [50, 51]. Further, while the lattice matching requirements in thin-film growth severely limits the available bandgap combinations in multijunction cells (Chapter 2.1.1), these restrains are thus alleviated in the nanowire geometry.

Third, nanowires can be synthesized by a novel technique called Aerotaxy [52, 53]. Here, the nanowires are synthesized at very high growth rates, from aerosol metal particles in a continuous stream of gas. This entirely removes the need for an epitaxial growth substrate, while also removing the costly batch-based synthesis methods used in conventional III-V growth.

Fourth, the nanowire geometry might also offer a benefit in terms of solar cell *PCE* compared to planar devices. Optical modelling has indicated that the nanowire geometry can modify the absorption and/or emission angles, reducing the entropy losses described in Chapter 2.1.1 and boosting the theoretical limits to the V_{OC} [54–56]. For certain conditions, a nanowire solar cell can therefore have a higher efficiency limit than a planar cell [54, 55]. While such photonic advantages are interesting, the devices currently realized experimentally are still mostly limited by electronic factors.

2.3 Design of a nanowire solar cell

Motivated by the potential benefits offered by the nanowire geometry, as outlined in Chapter 2.2, large research efforts have been invested in the field of nanowire solar cells over the last decade. Paper I review this body of research, and summarize guidelines for how a nanowire solar cell should be designed. In line with these guidelines, all work in this thesis has been based around a target structure sketched out in Figure 2.7, and outlined in the following bullet points.

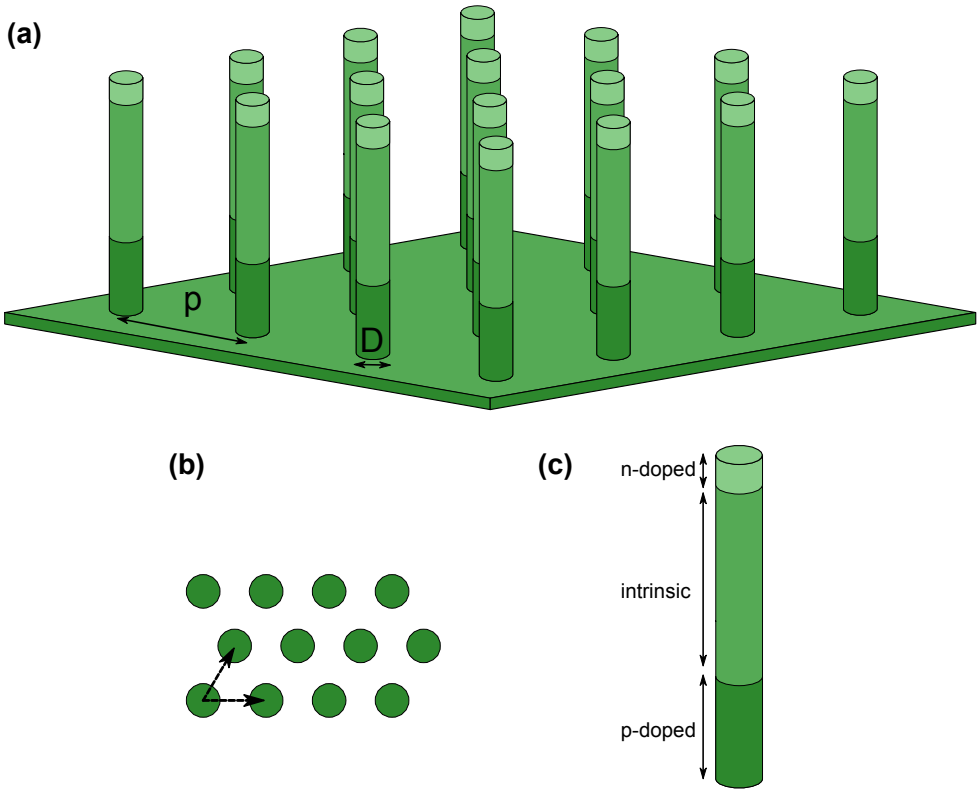


Figure 2.7 Schematic illustration of the target nanowire solar cell structure of this thesis: (**a**) A regular array of nanowires, having D = 180-200 nm and p = 500 nm. (**b**) A hexagonal array symmetry, shown in top view. (**c**) Each nanowire contains three differently doped segments, with a short *n*-doped segment on top, a long intrinsic segment in the middle, and a *p*-doped segment at the bottom.

- The nanowires themselves have a diameter, D, of 180-200 nm, exploiting diameter dependent resonances to give optimal sunlight absorption for InP [47](Paper I). The nanowires are placed in an array with hexagonal symmetry (Figure 2.7b), to ensure homogeneous conditions for all nanowires during growth. The nanowire array pitch, p, is 500 nm, giving a reasonable trade-off between light absorption [47] and pattern preservation during synthesis (Paper II, and Chapter 3.4.1).
- The nanowires have an axial junction, containing three segments of different doping (Figure 2.7c): the bottom segment is *p*-type, the middle segment is intrinsic, while the top segment is *n*-type. The middle intrinsic segment is included to improve carrier collection, as discussed in Chapter 2.1.2. However, the long intrinsic segment might incur a penalty in V_{OC}, thus

should be removed if long enough diffusion lengths in the material can be achieved.

- The top *n*-segment has been kept short (~70 nm), to minimize photogeneration in this high recombination segment [57].
- To minimize series resistance, we would like to have good contacts to the top and the bottom of the nanowires. To facilitate this, the top *n*-segment and the bottom *p*-segment should be highly doped, to reduce contact resistance to the transparent conductive oxide top contact and the growth substrate bottom contact.
- To limit recombination and ensure long diffusion lengths in the nanowires, we would ideally like to have a well-controlled crystal structure, a low density of bulk defects, and a well-passivated surface.
- The studies in the thesis have dealt with nanowires made of InP and/or $In_xGa_{1-x}P$, giving bandgaps appropriate for both single junction (Figure 2.7a) and double junction (Figure 2.8) architectures.

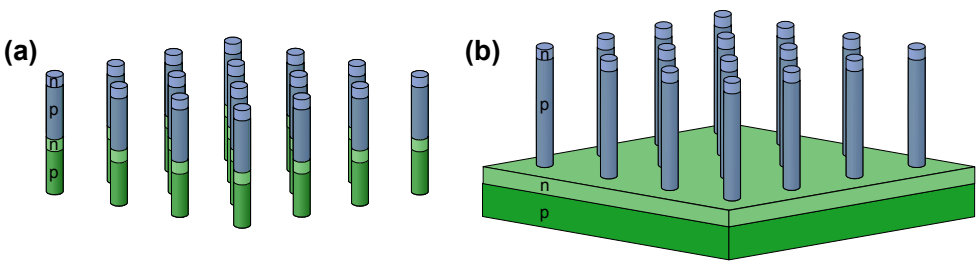


Figure 2.8 Schematic illustration of two basic nanowire tandem solar cell structures. (**a**) Arrays of heterostructured nanowires consisting of two materials of different bandgaps, each material consisting of a *p*-*n* junction. (**b**) Arrays of *p*-*n* junction nanowires on top of a planar solar cell. Blue and green indicate different materials, blue having the higher bandgap. These two basic structures can be expanded and/or combined to achieve more than two junctions.

All studies in this thesis have been performed with the aim of understanding and optimizing different parts of the target structure outlined above. However, the synthesis is challenging in many ways, especially when attempting to simultaneously control several different parameters (e.g. doping, crystal structure and surface passivation). To understand where the challenges lie, we need to first look into details of how the nanowire arrays are synthesized. An introduction to nanowire array synthesis is the topic of the next chapter, which will end with a discussion of some specific challenges in synthesizing the target structure described above.

3 Nanowire array synthesis

The methods to synthesize nanomaterials can be divided into two broad categories: top-down and bottom-up approaches. In a top-down approach, one starts with a bigger piece of material from which material is selectively removed in a more or less controlled manner, until the nanostructure(s) remains. In a bottom-up approach on the other hand, one starts with the building blocks of the nanostructure, atoms or molecules, and create an environment where they will themselves organize into the desired nanostructure. For nanowires, an example of top-down synthesis is to etch them out by reactive ion etching (RIE) from a piece of bulk material, by masking parts of the surface with an etch resistant material [58, 59]. However, the benefits offered by the nanowire geometry (discussed in Chapter 2.2) are largely lost when using a top-down approach. Therefore, the work in this thesis has focused on bottom-up nanowire synthesis.

A range of methods exist to synthesize nanowires bottom-up, or to "grow" nanowires as it is commonly called. The nanowires in this thesis are synthesized by *gold particle seeded vapor-liquid-solid (VLS) growth by metal organic vapor phase epitaxy (MOVPE).* This name distinguishes the method from others by defining the growth technique (MOVPE), the growth mode (VLS), and the factor that is facilitating the one dimensional growth, creating the wire-like structure (gold particle seeding). To understand how nanowires can be synthesized, it is necessary to discuss each of these terms in some detail. It is appropriate to start with an introduction of crystal growth by MOVPE, before returning to the specific use for nanowire synthesis. Thereafter, we will discuss the synthesis of ordered nanowire arrays by combining bottom-up growth with top-down lithographic techniques. In the final part of the chapter, we will introduce some growth challenges to be considered when growing nanowire arrays for solar cells.

3.1 Metal organic vapor phase epitaxy

Semiconductor devices, both bulk and nanoscale, are designed to transport, interact with and/or confine charge carriers and photons in a specific way. The more complex devices, such as lasers, light emitting diodes (LEDs) or multijunction solar cells,

contain several layers of different materials, with high demands on control of layer thickness, purity, and crystal quality. Epitaxial growth is typically the synthesis method of choice to create such devices.

The term *epitaxy* is derived from the Greek words epi ("upon" or "over") and taxis ("order" or "arrangement"), and refers to the growth of a crystal on top of another crystal, where the underlying crystalline substrate dictates the atomic arrangement of the growing material. This is in contrast to non-epitaxial growth, where the atoms are arranged independently of the substrate on which they are deposited, as in chemical vapor deposition (CVD) or sputtering methods. Nanowires can also be grown non-epitaxially, but we will only focus on the epitaxial growth methods in this thesis. If the material being epitaxially grown is the same as in the underlying crystal, it is called homoepitaxy, while if they differ, it is called heteroepitaxy.

In metal organic vapor phase epitaxy, the atoms to the growing crystal are supplied as metal organic molecules in the vapor phase, hence the name. Epitaxial growth can also be done by techniques where the precursor is supplied in a different chemistry or phase, such as hydride vapor phase epitaxy (HVPE), molecular beam epitaxy (MBE), or liquid phase epitaxy (LPE). Each of these techniques has their strengths and weaknesses. As the technique used in this thesis, all discussion of crystal growth will in the following be done with reference to MOVPE, even though many of the concepts discussed are generally applicable also to other growth techniques. For epitaxial growth to take place, conditions must be favorable for atoms from the vapor phase to incorporate into the solid phase at lattice sites determined by the substrate. In the following, we will discuss the necessary conditions for growth to take place, starting with the thermodynamic driving force.

3.1.1 Thermodynamic driving force

A process is thermodynamically favorable if it lowers the Gibbs free energy, G, of the system. A useful parameter to keep track of changes in Gibbs free energy is the chemical potential, μ, which can be written for component i in the system as,

$$\mu_i = \left(\frac{\partial G}{\partial n_i}\right)_{T,P,n_{j\neq i}} \quad \textbf{3.1}$$

where n_i is the number of moles of component i, T is temperature, and P is pressure. In MOVPE we want to move atoms from the vapor phase, v, to the crystal phase, c, and for this to yield a lowering of Gibbs free energy it follows from Equation 3.1 that $\mu_v > \mu_c$. Accordingly, growth is induced by increasing μ_v, achieved by supplying precursor gas at a concentration higher than the equilibrium concentration, i.e. supersaturating the vapor with growth species. The difference in chemical potential between the two phases, $\Delta\mu_{vc} = \mu_v - \mu_c$, is the thermodynamic driving force for the

reaction. A key advantage of vapor phase epitaxial techniques is the ease with which this driving force can be maintained, by constantly resupplying precursor gases to retain supersaturation as the reaction proceeds.

3.1.2 Mass transport and kinetics

The overall process of moving material from the vapor phase to the solid phase, with the total chemical potential difference $\Delta\mu_{vc}$, is divided into a number of different steps, each associated with its own chemical potential difference. These steps can be grouped into mass transport processes happening mainly in the gas phase (Figure 3.1a, green zone), and kinetic processes happening mainly at the crystal-vapor interface (Figure 3.1a, red zone). These processes are hard to model in detail, and can involve a large number of sub-reactions and -species. However, more broadly it is interesting to know whether kinetic or mass transport processes are limiting the growth. A distinction can be made by studying the temperature dependence of the growth rate. This is possible since the growth rate will be governed by the slowest process in the chain, and mass transport and kinetic processes have different temperature dependencies.

Kinetic processes include the release of the precursor atoms from the precursor molecule through thermal decomposition (pyrolysis), the migration of growth species on the crystal surface, and the formation of nuclei. Even though pyrolysis can happen in the gas phase, it is typically more likely at the crystal-vapor interface (Figure 3.1a, red zone), where also the other kinetic processes take place. The kinetic processes are thermally activated, thus follow an Arrhenius dependence, $exp(E_a / kT)$, and are at low growth temperature governing the growth rate (Figure 3.1c, red zone). In that case, the largest part of the total drop in chemical potential, $\Delta\mu_{vc}$, will happen at the crystal-vapor interface (Figure 3.1b, red line), and we are in what is referred to as the kinetically limited growth regime. Nanowires are typically grown in the kinetically limited growth regime, as kinetic limitations to growth are essential in obtaining the wire-like structure, discussed in more detail in Chapter 3.2. It should be emphasized that the kinetic processes involved in MOVPE are highly complex. For instance, the pyrolysis of common precursor molecules often does not only have strong temperature dependence, but is also strongly affected by the presence of other precursor gases, and/or the nature of the substrate surface. A review of precursor pyrolysis can be found in references [60, 61]. Further, note that there might be different kinetic processes that limit the growth in different systems or in different temperature ranges.

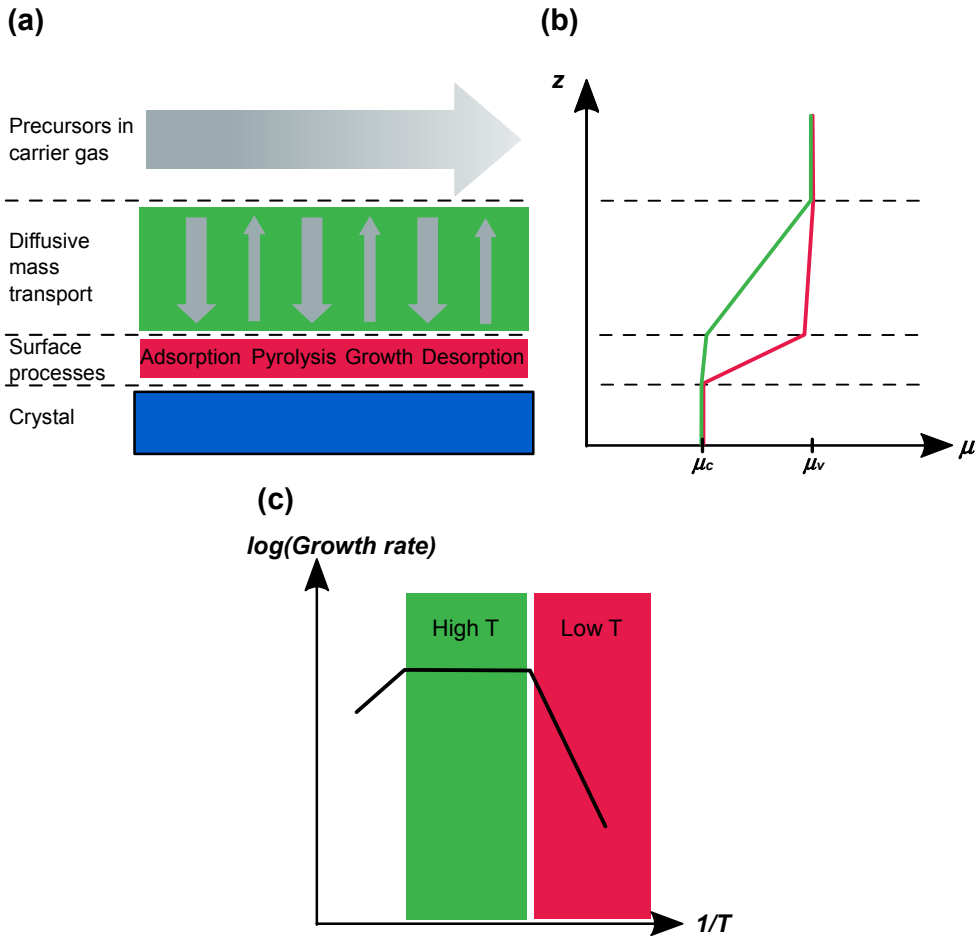


Figure 3.1 Schematic illustration of the difference in mass transport (green) and kinetic (red) processes in MOVPE according to (**a**) where they take place, (**b**) the corresponding chemical potential profile for the species limiting growth, and (**c**) their temperature dependence. Increasing growth temperature further from the mass transport limited growth regime, the growth rate will decrease, due to parasitic deposition on the reactor walls and enhanced desorption, lowering the supersaturation in the gas phase. Figure is adapted from Figure 7.12 and 7.13 in ref. [62].

Mass transport processes mainly include the transport of precursor molecules in the gas phase to reach the growth interface. This happens by diffusion through a boundary layer, typically modelled to consist of stagnant gas, close to the growth interface (Figure 3.1a, green zone). The diffusion is mainly driven by the concentration gradient established as the precursors decompose and growth species are removed by incorporation into the crystal. At high temperatures, the rate of the thermally activated kinetic processes is fast. The growth rate will therefore depend on

the rate of the mass transport processes, which have only weak temperature dependence (Figure 3.1c, green zone). Then, the largest part of $\Delta\mu_{vc}$ will fall over the boundary layer (Figure 3.1b, green line), and we are in what is referred to as the mass transport limited growth regime.

3.1.3 Nucleation theory

An important step in the growth process is the formation of nuclei in the initial stages of the growth. We will look into classical nucleation theory and consider a simple yet instructive model of a nucleus (Figure 3.2), in the form of a cylinder with radius r and height h, grown homoepitaxially with the top surface of the nucleus being identical to the substrate surface, and disregarding facet dependence of the interface energies or any strain effects.

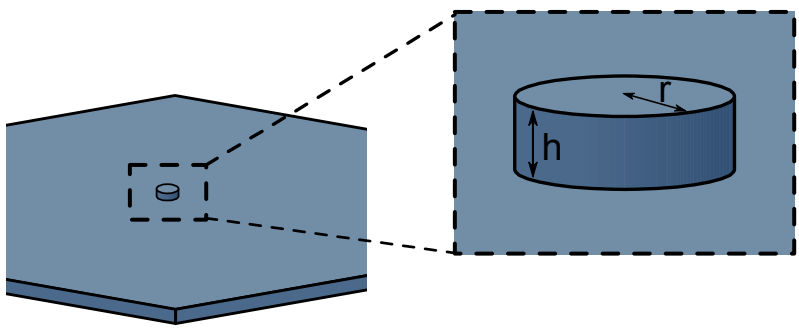


Figure 3.2 Simple model of a homoepitaxial nucleus, in the form of a cylinder with radius r and height h.

The change in Gibbs free energy for creating such a nucleus, ΔG_N, can then be written as

$$\Delta G_N = -\Delta\mu_{vc}\frac{h\pi r^2}{V_{m,c}} + 2\pi r h\gamma_{vc} \qquad \textbf{3.2}$$

where $V_{m,c}$ is the molar volume of the crystalline phase, and γ_{vc} is the interface energy between the vapor and the crystal phase. Equation 3.2 shows how creating a nucleus energetically is a competition between two terms: the energy gain of moving material into the phase of lower chemical potential (first term), and the energy cost of creating interfaces (second term). The interface energy comes from the change in chemical bonding when creating the interface, and will vary depending on factors such as the phases present, crystal orientation, adsorbed species, and/or surface reconstruction. For small nuclei, the energy cost of creating these interfaces will outweigh the driving

force of the supersaturation. These small nuclei can lower the Gibbs free energy by decreasing their size, and are thus not stable. However, a critical nucleus radius, r^*, exist, where the chemical potential term will start to dominate (due to its r^2 dependence), lowering the Gibbs free energy as the nucleus continues growth (Figure 3.3). This critical radius can be found by solving $d\Delta G_N/dr = 0$ for Equation 3.2. For our model, we get

$$r^* = V_{m,c} \times \frac{\gamma_{vc}}{\Delta\mu_{vc}} \qquad \textbf{3.3}$$

The change in Gibbs free energy at this critical nucleus radius can be seen as the activation energy of nucleation, typically referred to as the nucleation barrier, ΔG_N^*:

$$\Delta G_N^* = h\pi V_{m,c} \times \frac{\gamma_{vc}}{\Delta\mu_{vc}} \qquad \textbf{3.4}$$

Thus the critical radius (Eq. 3.3) and the nucleation barrier (Eq. 3.4), are set by the balance between interface energies and the supersaturation. For example, a higher supersaturation (Figure 3.3a) or a lower interface energy (Figure 3.3b), yield a smaller critical radius, a lower nucleation barrier and hence a higher rate in the formation of stable nuclei. We will return to these concepts in the discussion of nanowire growth, in Chapter 3.2.

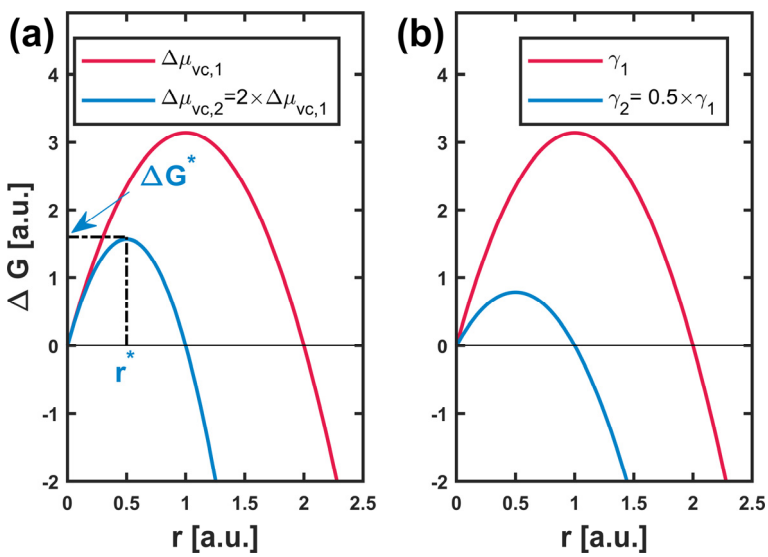


Figure 3.3 Change of Gibbs free energy as a function of nucleus radius for (**a**) two different values of $\Delta\mu_{vc}$, and (**b**) two different values of γ. In (a), the nucleation barrier ΔG^* and critical radius r^* for $\Delta\mu_{vc,2}$ are indicated by the dashed lines. ΔG^* and r^* can be found in the same manner for the other examples shown.

3.1.4 The MOVPE reactor

Practically, the growth facilitating conditions in the MOVPE chamber are set by controlling substrate temperature, chamber pressure, and the flow of precursor and carrier gases. Designing the MOVPE chamber to provide control of these parameters is a comprehensive engineering challenge, and the reader interested in details is referred to reference [63]. For the purpose of the discussion in this thesis, it is sufficient to specify some relevant details of the MOVPE reactor used. All experiments were carried out in an Aixtron 200/4 MOVPE, using 100 mbar working pressure, H_2 as a carrier gas in a horizontal-flow reactor geometry, and with the sample placed on a rotating graphite susceptor heated by halogen lamps and temperature control through a thermocouple system.

3.2 Basics of particle seeded nanowire growth

Almost sixty years ago, researchers from Bell Laboratories reported observations of elongated wire-like Si crystals (called "whiskers" in the original work) when certain metal impurities were present in the growth chamber [64, 65]. In 1964, two of the researchers, Wagner and Ellis, published a paper where they presented a model to explain these observations, termed the vapor-liquid-solid (VLS) growth model [66]. According to the VLS model, growth constituents from the vapor are incorporated into the solid by first dissolving in and forming a liquid alloy with a metal seed particle. Since Wagner and Ellis' work the details of the VLS model have been developed and discussed substantially, and it has been used to explain growth in a wide range of materials and growth systems. Excellent reviews of this development can be found in papers by Dick [67] and Wacaser et al [68]. Based on the comprehensive discussions by these authors, we will in the following present some key arguments and insights that have led to the current understanding of particle seeded nanowire growth. Note that expansions of the VLS model have been used to explain growth also when the supply or seed particle phases are different, such as in vapor-solid-solid growth (VSS) [69, 70] or solution-liquid-solid growth (SLS) [71]. Also, a range of different metals have been studied as seed particles [72], including what is called self-seeded growth, where e.g. Ga particles are used to grow GaAs nanowires [73]. The following discussion will be made in terms of gold seeded VLS growth, even though the reasoning is not dependent on the exact phases or materials involved.

To grow elongated nanowire structures it is required that the growth rate in certain locations on the substrate is much higher than in all other locations, including on the sidewalls of the growing nanowire. Thus, to understand metal seeded nanowire growth, the key question to answer is why the metal particle, in so many different

systems, is able to bring about such a growth rate enhancement. For material from the vapor phase to dissolve in the liquid particle, we need to have a chemical potential difference $\mu_v > \mu_l$, and similarly $\mu_l > \mu_c$ must hold for material to precipitate from the liquid phase into the crystal phase. However, this gives $\mu_v > \mu_l > \mu_c$, thus the supersaturation between vapor and crystal phase is bigger than between liquid and crystal phase, $\Delta\mu_{vc} > \Delta\mu_{lc}$. Hence, from a thermodynamic perspective there should not be a growth rate enhancement underneath the seed particle as compared to the plain crystal surface. It has been argued that there might still be an enhanced supersaturation locally due to the seed particle acting as a catalyst for pyrolysis. Even though this might play a role in some systems [74–76], it cannot be used as a general model to explain nanowire growth [67, 68]. Instead, as described in detail by Wacaser et al [68], we need to consider the kinetics of nucleation.

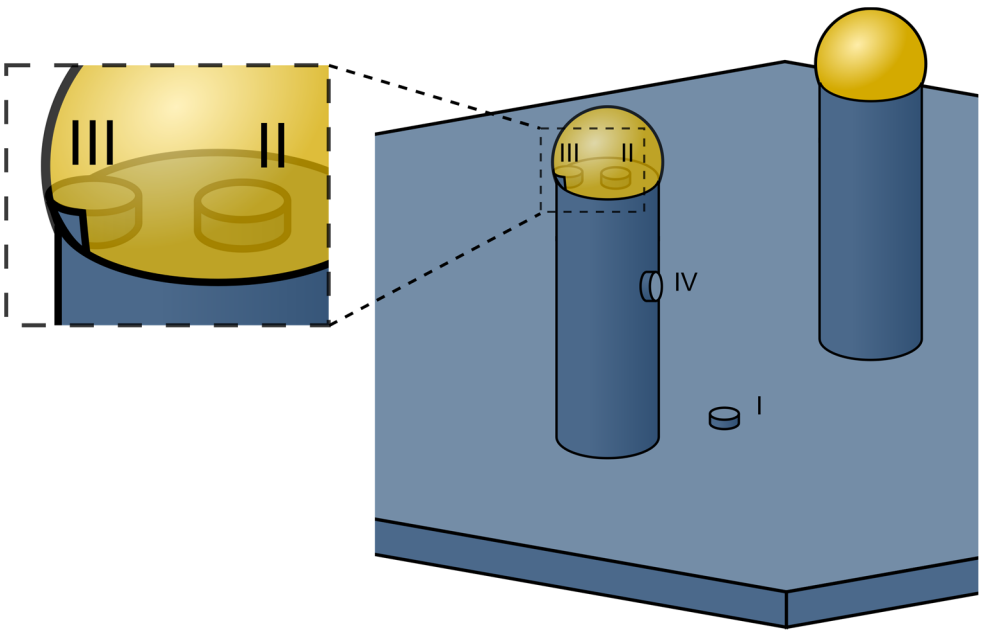


Figure 3.4 Schematic showing different possible sites of nucleation in a nanowire growth system: (I) on the bare substrate surface, (II) at the seed particle-nanowire interface, with all sides of the nucleus interfacing with the seed particle, (III) at the triple-phase boundary, with the sides of the nucleus interfacing partly with the vapor and partly with the liquid, (IV) on the nanowire side facet.

Let us consider two of the possible sites of nucleation in a nanowire growth system, indicated in Figure 3.4; on the flat surface (I), and underneath the metal particle (II). We model the nuclei analogous to what we did in Chapter 3.1.3, and the change of Gibbs free energy in their formation can be given as:

$$\text{(I)} \quad \Delta G_{N,I} = -\Delta\mu_{vc}\frac{h\pi r^2}{V_{m,c}} + 2\pi r h\gamma_{vc}$$
$$\text{(II)} \quad \Delta G_{N,II} = -\Delta\mu_{lc}\frac{h\pi r^2}{V_{m,c}} + 2\pi r h\gamma_{lc} \qquad \textbf{3.5}$$

Correspondingly, the nucleation barrier at the two different positions will be:

$$\text{(I)} \quad \Delta G^*_{N,I} = h\pi V_{m,c} \times \frac{\gamma_{vc}}{\Delta\mu_{vc}}$$
$$\text{(II)} \quad \Delta G^*_{N,II} = h\pi V_{m,c} \times \frac{\gamma_{lc}}{\Delta\mu_{lc}} \qquad \textbf{3.6}$$

For nucleation kinetics to give an increased growth rate in position II compared to position I, position II needs to have the lower nucleation barrier, $\Delta G^*_{N,II} < \Delta G^*_{N,I}$. As discussed above, we have $\Delta\mu_{lc} < \Delta\mu_{vc}$, hence Equation 3.6 shows that a lower nucleation barrier must be due to a lower interface energy between the liquid and the crystal phase than between the vapor and the crystal, $\gamma_{lc} < \gamma_{vc}$. This alone could explain preferential nucleation under the seed particle in many systems. However, an even lower nucleation barrier is typically found when forming a nucleus where the solid, liquid and vapor phases meet (Figure 3.4, position III), at what is called the triple phase boundary [68, 77]. Here, parts of the crystal-liquid interface of the nucleus are replaced by a crystal-vapor interface, which also replaces parts of the liquid-vapor interface of the particle. This site is preferential since the nucleus can adjust its shape to lower the interface energy contributions as much as possible [68]. In summary, it is now generally accepted that the seed particles allow nanowire growth by providing kinetically preferential sites of nucleation, enhancing growth rates underneath the seed particle.

As soon as a stable nucleus has formed, addition of atoms to the edge-sites of this nucleus proceeds without an energy barrier, since no new interfaces are created. Therefore, as long as the diffusivity of adatoms in the seed particle is sufficiently high, the supersaturation of the particle will drive material to be added quickly at these sites, until the layer is completed. This rapid crystallization of material lowers the supersaturation in the particle, which again increases the nucleation barrier (Eq.3.6, Figure 3.3a). An incubation time follows where the particle regains its supersaturation by resupply of growth species, until the higher supersaturation makes another nucleation event likely [78]. Thus, the growth proceeds through a mechanism similar to birth and spread in planar growth, adding one monolayer at a time to the growing nanowire. A schematic illustration of this process is shown in Figure 3.5.

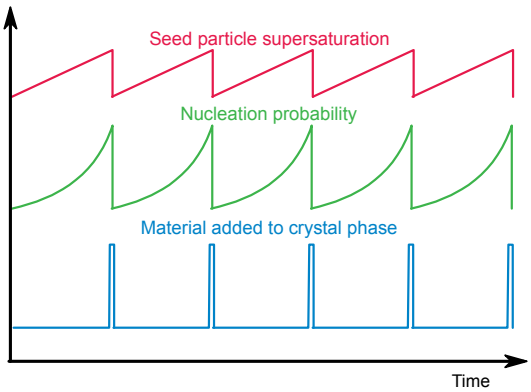


Figure 3.5 Schematic of how seed particle supersaturation, the corresponding nucleation probability, and the resulting amount of material added to the crystal phase might vary with time. Adapted from Fig.4.22 in [79].

3.3 Growth substrates

Most epitaxial nanowire growth has so far taken place on native substrates, i.e. Si nanowires have been grown on Si, GaAs have been grown on GaAs etc. However, nanowire growth is possible also on various foreign substrates (enabled by relaxed lattice matching requirements in the nanowire geometry, discussed further in Chapter 3.4.3). This is especially interesting for the III-V materials, where the typically expensive growth substrates constitute a major part of the manufacturing cost. A significant effort has been made in growing III-V nanowires on foreign substrates such as Si [80–83], graphene/graphite [84–86] and SiO_x/glass [74, 87–89]. The growth on Si is especially interesting due to the prospects of integrating the excellent optical properties of III-Vs with Si electronics.

Nanowire array optoelectronic devices, such as the solar cells discussed in this thesis, are usually made from nanowires grown vertically with respect to the growth substrate. Tuning the nanowire growth to proceed along various crystal directions is possible to a certain extent by tuning factors such as growth temperature, V/III-ratio or nanowire diameter (by changing initial seed particle size) [90]. Normally however, nanowires grow along the low energy (111) (for ZB) or (0001) (for WZ) directions, and the easiest way to achieve vertical arrays is therefore to grow from (111) substrates.

The target structure in this thesis work has been nanowires with a *p*-type bottom segment (Figure 2.7). Therefore, all nanowires presented here have been grown from

InP:Zn (111)B substrates, with a high doping concentration of 5×10^{18} cm^{-3} to allow the substrate to be used as an Ohmic back contact to the *p*-type nanowire segment. The wafers used for epitaxial growth are supplied so called "epi-ready", meaning that the semiconductor surface is protected by a specially designed oxide. However, for epitaxial growth to take place, the supplied growth species (and for seed particle assisted nanowire growth, the seed particle) need to have access to the semiconductor surface. In this thesis the oxide has been removed solely by an in situ annealing step prior to nanowire growth, specified in the experimental section of each paper.

3.3.1 Substrate patterning for ordered array growth

A number of different methods have been used to deposit seed particles used in the VLS method, with different strengths and weaknesses [91, 92]. For nanowire array devices, it is desirable that the deposition method gives control of both seed particle position and size. By growing from a periodic and uniform array of seed particles, all nanowires in the array will experience similar growth conditions (not considering edge-effects), of central importance to produce a nanowire array with high uniformity in parameters such as nanowire length, doping profiles, and shell thickness. Controlling the size of the seed particle provides control of the nanowire diameter, which is central to maximize light absorption in the array (Paper I). The technique used most extensively so far to produce ordered seed particle arrays is electron beam lithography (EBL) [93]. Despite its slow sequential pattern writing, EBL is useful in a research setting due to its large flexibility in pattern design. However, for large area devices such as solar cells, a method with higher throughput is desirable. In this respect, nanoimprint lithography (NIL) has proven useful. NIL is the only patterning technique used in this thesis, and will be discussed more thoroughly below. Other patterning techniques are also interesting to produce seed particle arrays for large area ordered nanowire growth, such as laser interference lithography [94, 95], nanosphere lithography [96, 97], and displacement Talbot lithography [98].

Nanoimprint lithography

Nanoimprint lithography (NIL) was first presented by Chou et al. in 1995 [99, 100], and has since then advanced significantly towards industrial competitiveness [101]. With this technique, a nanostructured pattern is transferred from a stamp to a polymer by means of physical contact and material displacement. The pattern-features are transferred from the stamp to the polymer simultaneously over the stamp area, allowing for full wafers to be imprinted in one step. Further transfer of the pattern into or onto the underlying material is done by using the polymer as a stencil, as is commonly done in other lithographic techniques. Defining patterns for nanowire array synthesis by NIL was first done in 2004 by Mårtensson et al. [102]. In this thesis, formation of a seed particle array on the growth substrate was formed by a

NIL process based on technology from Obducat AB [103]. Each step in the pattern formation process is described in the following, and illustrated in Figure 3.6.

First, an intermediate polymer stamp (IPS) is created from a master nickel stamp. The IPS constitutes a UV-transparent stamp, flexible to conform to surface roughness and/or curvature, and reduces the wear on the more expensive master stamps, made by EBL [103]. The IPS film is placed on top of the master stamp and heated above its glass transition temperature (Figure 3.6a), before high pressure is used to force the flow of IPS polymer to conform to the pattern of the underlying master stamp (Figure 3.6b). In this way, the IPS forms a negative of the master stamp pattern, thus having a periodic array of pillars at the positions of the depressions in the master stamp (Figure 3.6b). After formation of the IPS, the wafer to be imprinted (for the work in this thesis, always a 2'' InP:Zn (111)B wafer) is covered by a double layer resist (Figure 3.6c), using spin-coating and curing of first LOR0.7A and then TU7-120. These two resists will for simplicity be referred to as bottom-layer and top-layer resist, respectively. The IPS is put on top of the substrate with the double-layer resist, before heat is applied to reach a temperature higher than the glass transition temperature of the top-layer resist (Figure 3.6d). At this temperature, pressure is applied uniformly on top of the IPS, driving the top-layer resist to flow from underneath the pillars in the stamp, to the voids between the pillars. Thus, a pattern resembling the original master stamp is formed; a periodic array of depressions in the top-layer resist at the positions of the pillars in the IPS (Figure 3.6e). By tuning the thickness of the top-layer resist, it is ensured that a thin layer of resist remains at the bottom of these holes, separating the bottom-layer resist from the IPS. For the established pattern in the resist to remain after demolding of the stamp, photocuring of the top-layer resist is done by exposure with UV-light through the transparent IPS (Figure 3.6f). After demolding (Figure 3.6g), the residual layer at the bottom of each hole is removed by homogeneously thinning the top-layer resist by O_2-plasma in a reactive ion etcher (RIE) (Figure 3.6h). Here, the etching time is optimized to open the holes to the underlying resist, but to leave sufficient thickness of the top-layer resist to still act as a mask during subsequent steps. A wet-chemical etchant (MF 319) is used to partly dissolve the bottom-layer resist, accessible for the etchant through the holes in the top-layer resist (Figure 3.6i). The isotropic nature of the dissolution process leaves an undercut profile. Next, gold is evaporated onto the underlying growth substrate through the holes in the double-layer resist (Figure 3.6j). Finally, the resists and surplus gold is removed in a lift-off process, leaving arrays of gold particles on the growth substrate (Figure 3.6k). In the lift-off process the bottom-layer resist is fully dissolved by use of remover 1165, and the wafer is thereafter cleaned in de-ionized water and dried, with no other treatment needed. With the exception of a few millimetres at the edge, the pattern of seed particles now fully covers the 2'' wafer, which is usually cleaved or sawed into smaller pieces used for growth experiments.

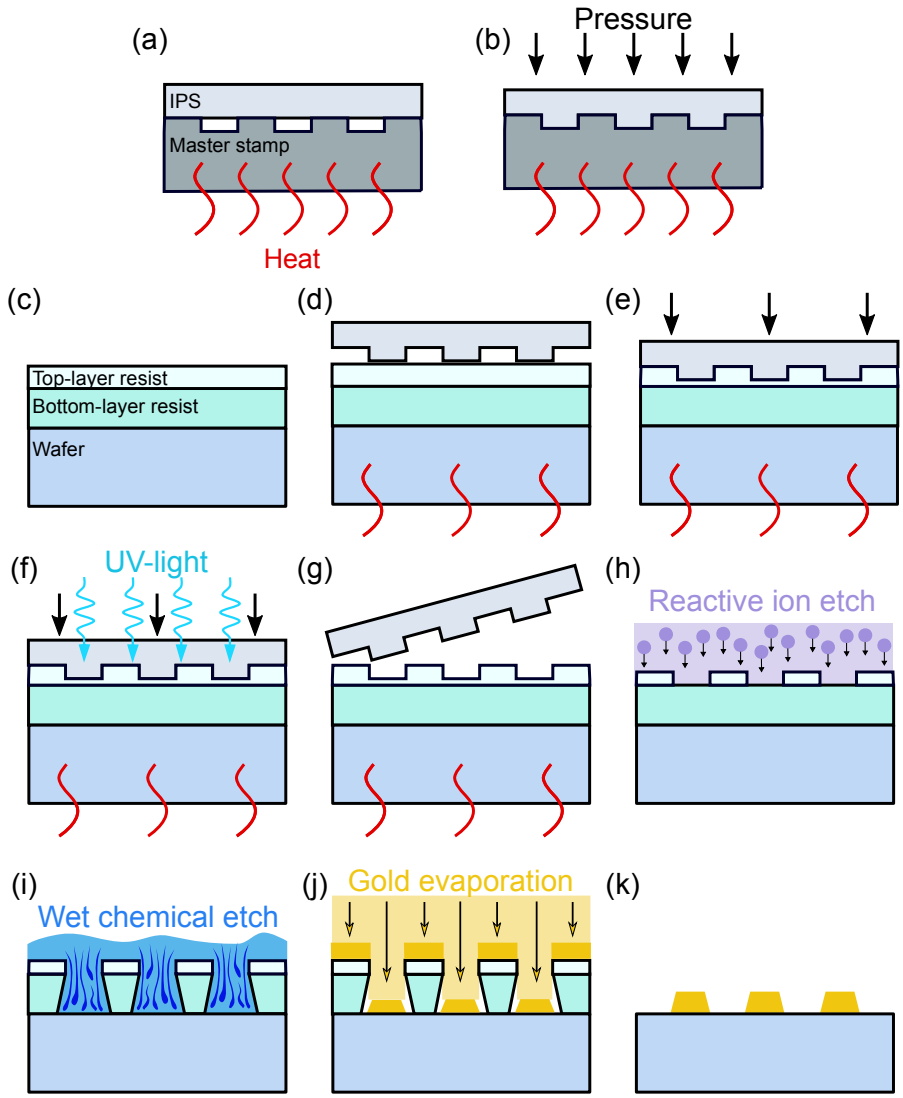


Figure 3.6 Schematic illustration of gold particle patterning of a wafer by nanoimprint lithography. Formation of an intermediate polymer stamp (IPS) from a master stamp by heating above the glass transition temperature of the IPS (**a**), and applying pressure (**b**). The wafer is covered by a double layer resist (**c**) before put in contact with the IPS and heated (**d**). Pressure is applied (**e**), a negative of the IPS is formed in the top-layer resist, before it is cured by UV-light (**f**), and the IPS is demolded (**g**). Reactive ion etching is used to open up holes in the top-layer resist (**h**) before a wet-chemical etch step is used to form an undercut profile in the bottom-layer resist (**i**). Gold is evaporated onto the wafer through the holes in the resist (**j**), before the double layer resist and excess gold is removed in a lift-off step, leaving an array of gold particles on the wafer surface (**k**), in a pattern as defined by the master stamp.

The process of pattern formation by NIL described here is well established in our lab, and as long as proper maintenance of the process is done, it is used routinely to create patterns with high yield (>99.9%, an example is shown in Figure 3.7a). The low density of missing seed particle that do exist is most likely related to defects in the stamp, such as a somewhat too short pillar in the IPS. For all substrate patterning in this thesis a stamp was used yielding a hexagonal pattern of seed particles (Figure 3.7b), with a diameter of approximately 190 nm and a pitch of 500 nm (giving a density of 4.65 particles/μm^2). The hexagonal symmetry was chosen to give all nanowires an equal collection area for diffusing growth species, while the pitch and the diameter was chosen according to the target nanowire solar cell structure described in Chapter 2.3. The nanowire diameter can be tuned by changing the seed particle volume, which in the NIL procedure is easily obtained by changing the thickness of gold evaporated onto the surface (Figure 3.6j).

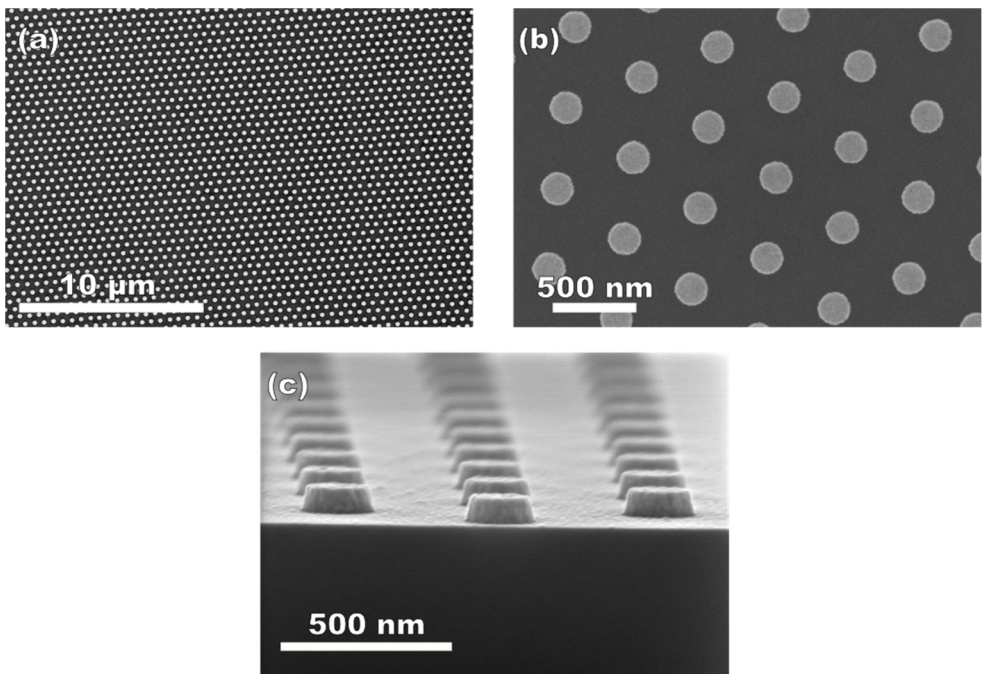


Figure 3.7 Scanning electron microscope images of gold particle pattern created by nanoimprint lithography. (**a**) Zoom-out top-view, indicating the long range high pattern fidelity in the pattern transfer process. (**b**) Top-view and (**c**) cross-section view showing the particles in the form of gold discs placed in a hexagonal pattern.

3.4 Some growth considerations for nanowire solar cells

As introduced in Chapter 2.3, significant knowledge has accumulated on how a nanowire solar cell should be designed to achieve high performance. At this point, the main challenge is to use the techniques described in this chapter to controllably synthesize nanowire arrays according to these design guidelines, and further process them into solar cells. In the remainder of this chapter, we will briefly introduce some of the most important challenges in terms of growth and relate them to the work done in this thesis. Note that these topics are reviewed also in Paper I, in the broader context of the overall literature in the field.

3.4.1 Pattern fidelity through stages of nanowire array growth

Even though the NIL procedure described in Chapter 3.3.1 produces high yield patterns of seed particles (Figure 3.7), it is not always trivial to translate this pattern into an ordered array of nanowires. For instance, it has been reported in the literature that special cleaning might be needed to avoid growth of small parasitic nanowires between the designated growth centers [104]. However, for our process this has not been a significant problem, and the major challenge has instead been displacement and coalescence of the gold particles prior to nanowire growth. An example of a growth experiment where this problem was significant can be seen in Figure 3.8 a-b. We observe that displacement and merging of gold seed particles at some point before nanowire nucleation led to a large number of thicker nanowires. Besides destroying the pattern designed for good light absorption and uniform growth conditions, the resulting uneven lengths of the nanowires are problematic in the subsequent processing into solar cells. The degree of displacement and coalescence also varied significantly between different wafers, complicating the task of making reproducible experiments. Understanding and addressing this problem of severe particle displacement was the topic of Paper II, and resulted in three different strategies to improve pattern fidelity through the stages of nanowire growth. Implementing these strategies has been key in enabling the research presented in this thesis, allowing dense nanowire arrays to be reproducibly grown with high pattern fidelity (Figure 3.8 c-d). Specifically, the heat treatment before imprint combined with the pre-anneal nucleation (see Paper II for details) was used in Papers III-XI, while the SiN_x growth mask was used in Papers XII-XIII. Recently, a similar approach to the pre-anneal nucleation was adopted by another group, which also observed significant improvements in pattern preservation [105].

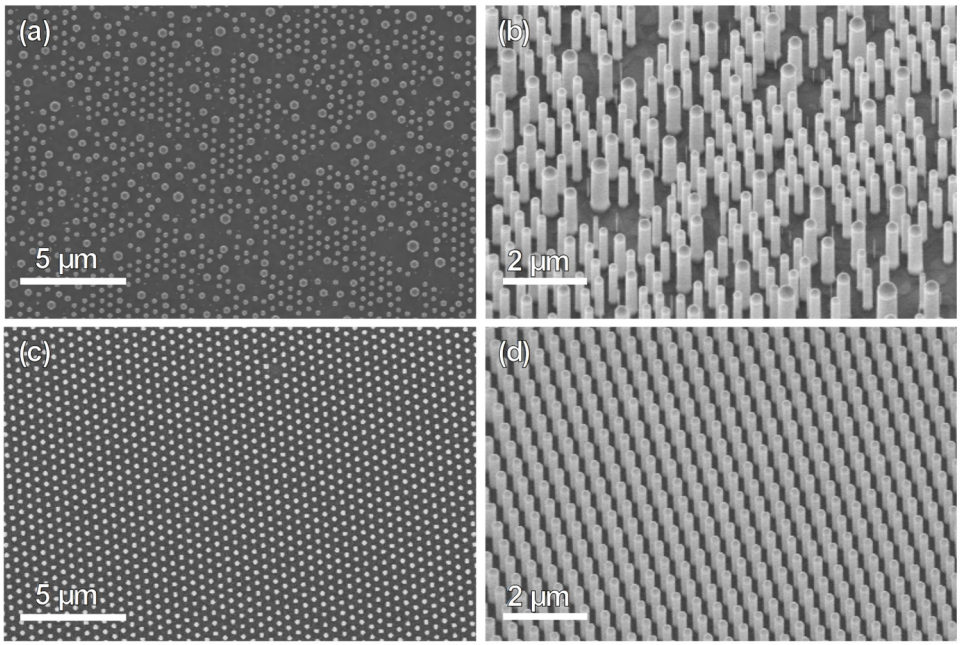


Figure 3.8 SEM images of nanowire arrays grown showing bad pattern preservation at (**a**) 0^0 tilt and (**b**) 30 ^{0} tilt, and showing good pattern preservation at (**a**) 0^0 tilt and (**b**) 30 ^{0} tilt.

3.4.2 Polytypism

The III-V materials (excluding the III-nitrides) in bulk form adopt the zincblende (ZB) crystal structure, as this is their thermodynamically favorable phase. It has therefore drawn significant attention that the same materials in nanowire form instead can adopt the metastable wurtzite (WZ) crystal structure, or more commonly a WZ-ZB mixture. To explain this, we again need to look at the kinetics of nucleation. The difference in the WZ and ZB structure can be seen as a difference in bilayer stacking sequence along the <111> axis, where WZ exhibit ABABAB.. stacking, and ZB exhibit ABCABC.. stacking. Analogous to how nucleation might happen preferentially under the metal particle as compared to on the bare substrate even if the latter is thermodynamically favorable (Chapter 3.2), a nucleus might take on a position relative to the previously grown layer corresponding to metastable WZ stacking if that has a lower nucleation barrier than the ZB stacking [77]. This can be the case if nucleation happens at the triple-phase boundary (position III in Figure 3.4) [77], supported by recent observations of GaAs nanowire growth in situ by TEM [106]. Here, the seed particle geometry was observed to dictate the nucleation position, and thereby the crystal phase.

In relation to solar cell performance, important to note is that the crystal structure can affect electrical transport and optical properties. For instance, ZB segments in otherwise WZ InP nanowires can act as electron traps [107]. In Paper X, such trapping was discussed as a likely reason for parts of the observed axial variation in carrier concentration. Different growth parameters have been reported to affect the crystal phase formation, such as growth temperature [108, 109], V/III-ratio [110–112] and impurity doping [113, 114] (Paper V-VI). Based on this, we can identify several factors likely to result in an axial variation of crystal structure in our InP nanowire solar cells. For example, the bottom *p*-segment was doped using DEZn, which induces ZB crystal structure in InP [113, 114], while the top *n*- segment was doped using TESn, known to have no considerable effect on the crystal structure. Further, the effective V/III ratio at the growth front varies during growth, since the supply of In species is limited by adatom surface migration (Paper V), lowering the group III supersaturation as the nanowire grows longer. It is reasonable to assume that the resulting variations in crystal structure along the length of the nanowires have an effect on solar cell performance. However, it has so far not been established if and how the crystal structure is/will be limiting, partly since the growth conditions used to tune the crystal structure as described above also has considerable effects on other material properties.

3.4.3 Doping

Controlled doping of the nanowire material is important to define the charge separating *pn*-junction in the solar cell (Chapter 2.1). Since the nanowires are grown in the VLS growth mode, in the presence of a metal catalyst, dopant incorporation can be quite different from that in thin-film epitaxy. Further, the growth dynamics can be strongly affected by introducing dopants. This was studied for $In_xGa_{1-x}P$ nanowires in Paper V, where we showed that doping using DEZn resulted in a smaller nanowire diameter, a more predominant ZB crystal structure, a more Ga-rich composition, and an increased axial growth rate. In contrast, doping $In_xGa_{1-x}P$ nanowires using TESn (Paper VI) gave no significant change in the growth dynamics, while using H_2S resulted in an increased growth rate, a more predominant WZ crystal structure and a more axially homogeneous composition as compared to the nominally intrinsic case. A thorough review of semiconductor nanowire doping can be found in ref. [115]. Quantitative characterization of doping levels in nanowires has been an important topic of this thesis work (Paper III-VI and IX-X), and is discussed further in Chapter 4.3.

3.4.4 Growing heterostructures

An important benefit of the nanowire geometry is the possibility to create heterostructures with reduced requirements on lattice matching. This allows for high-quality heterostructures of materials unavailable in planar growth [87, 116, 117], where the strain would build up and create dislocations (or result in 3D growth) if the layer exceeds a critical thickness. For nanowire solar cells, of special interest is the possibility to combine materials with bandgaps matched to the solar spectrum, as discussed in Chapter 2.2. To this end, different InP/$In_xGa_{1-x}P$ heterostructures containing a tunnel (Esaki) diode were grown and studied in Paper VII.

By shifting growth conditions from promoting axial to radial growth, core-shell structures with radially differing materials and/or doping can be created. Creating such structures is of interest to nanowire solar cells when creating radial junctions or surface passivating shells. A discussion of this is provided in Paper I, and could become important to provide surface passivation to our solar cells as discussed in Paper VIII, but has otherwise not been studied in this thesis.

3.4.5 Memory effects

Memory effects are of special concern both when changing dopants (Chapter 3.4.3) and when growing heterostructures (Chapter 3.4.4). The term is used to describe effects that can cause growth conditions during some part of a growth sequence to influence material grown later. From planar growth it is well known that a background pressure of certain materials can arise from physisorbed and/or chemisorbed species on e.g. the susceptor or substrate which lingers in the reactor before desorbing [118, 119]. In this way, elements can be incorporated into material grown a significant time after the corresponding precursor gas was switched off. Different growth species give rise to memory effects of differing degrees, but generally a low vapor pressure of the growth species leads to a strong memory effect and a high vapor pressure the contrary. In VLS nanowire growth, the metal catalyst introduces an additional type of memory effect, the so-called reservoir effect where material is stored in the metal particle [120]. For the gold seeded III-V nanowires, some of the elements (typically the group III element and some of the dopants) alloy with the gold seed particle, which can thus act as a reservoir of these elements even after switching of the precursor gases.

In this thesis, memory effects were of special concern in Paper VII, when growing different configurations of a *n*-InP/*p*-$In_xGa_{1-x}P$ heterostructure tunnel diode. To obtain a working tunnel diode, as indicated by a negative differential resistance (NDR) region in the *IV*-curve, the heterointerface should be sharp with degenerate doping on both sides of the *pn*-junction. Two out of four tested configurations

showed an NDR. Differences between the four configurations in terms of sharpness in heterointerface and tunnel diode characteristics was explained in terms of differences in memory effects between different group III (Ga and In) and dopant (Zn, Sn and S) elements.

Memory effects were also a concern when growing *p-i-n* InP nanowires, where high DEZn flow during the growth of the bottom *p*-segment seemed to alter the doping level in the nominally intrinsic segment grown afterwards, as discussed in Paper VIII.

3.4.6 Avoiding radial growth

To facilitate preferential interface nucleation (Chapter 3.2), growth conditions need to be carefully tailored. For example, the growth temperature should be kept in the kinetically limited growth regime (Chapter 3.1.2), to allow for nucleation to limit the growth. However, to a certain degree there will always be a competition between nucleation underneath the growth particle, and nucleation on the substrate surface and the nanowire sidewalls (Figure 3.4, position II-III, I and IV, respectively). For many growth conditions, this leads to significant deposition on the surface and the sidewalls, resulting in more cone-like than wire-like structures. For device applications this is often undesirable, and especially so for axial junction nanowire solar cells where tapering can lead to short-circuiting of the junction. Unfortunately, the growth parameter space where this can be sufficiently avoided is often quite limited. An important advance in the field has therefore been the development of in-situ etching to reduce tapering during nanowire growth [121, 122]. This etching widens the parameter space for non-tapered growth and grants larger freedom to optimize the growth also for other material properties. Further, it has been observed to reduce incorporation of carbon impurities [105, 121]. In this thesis, HCl has been used as an in situ etchant to avoid radial and substrate growth in the InP and $In_xGa_{1-x}P$ material systems (Papers III-XI).

4 Characterization

In the previous two chapters, we have described first how a nanowire solar cell should be designed, and thereafter the basics of nanowire array synthesis. To understand the connection between synthesis conditions, material properties and solar cell performance, a range of different characterization techniques might be useful. In this chapter, the characterization techniques used in this thesis are introduced.

4.1 In situ optical reflectometry

Optical reflectometry has been extensively used in this thesis to monitor the nanowire length and growth rate in situ. Optical reflectometry has been used to monitor thin film growth for decades, but was just recently adapted to monitor nanowire growth [123]. This was a significant advancement, as the tool-box for understanding nanowire growth by MOVPE is mainly consisting of post-growth characterization techniques. In Figure 4.1a, a reflectance spectrum from the growth of an InP nanowire array is shown in the wavelength range 400-800 nm. The interference fringes seen in the spectrum arise from destructive and constructive interference between light reflected from the top of the nanowire and light reflected at the nanowire-substrate interface. To convert these interference fringes to a nanowire length, L, we follow the procedure described in ref. [123]. First, minima and maxima for each wavelength, λ, are picked out and numbered, with the minima numbered as m = 1,3,5,… and the maxima numbered as m = 2,4,6,… (example shown in Figure 4.1b). Then L can be calculated as:

$$L = \frac{m \times \lambda}{4 \times n_{eff}(\lambda)} \qquad \textbf{4.1}$$

where $n_{eff}(\lambda)$ is an effective refractive index for the nanowire array. For our specific array pattern (described in Chapter 3.3) $n_{eff}(\lambda)$ was found from calibration runs: InP nanowires were grown, L was measured by scanning electron microscopy (see Chapter 4.2), and an effective refractive index for each wavelength was calculated by rearranging Equation 4.1. Values of $n_{eff}(\lambda)$ for our pattern was found as an average of 12 calibration runs and are plotted in Figure 4.1c. While InP nanowires were grown

in the calibration runs, we showed in Paper V how this $n_{eff}(\lambda)$ is valid also for growth of $In_xGa_{1-x}P$ for the studied composition range of $1 > x > 0.6$, containing interesting compositions for nanowire tandem solar cells. Figure 4.1d shows an example plot of the nanowire length as a function of time for an array of InP nanowire *p-i-n* structures, extracted from Equation 4.1 by use of $n_{eff}(\lambda)$ plotted in Figure 4.1c. This extraction procedure has been greatly simplified by use of a custom made Matlab program [124]. Typically, only data in the 500-700 nm wavelength range was used for length extraction, as this region shows the clearest and cleanest interference pattern for our samples.

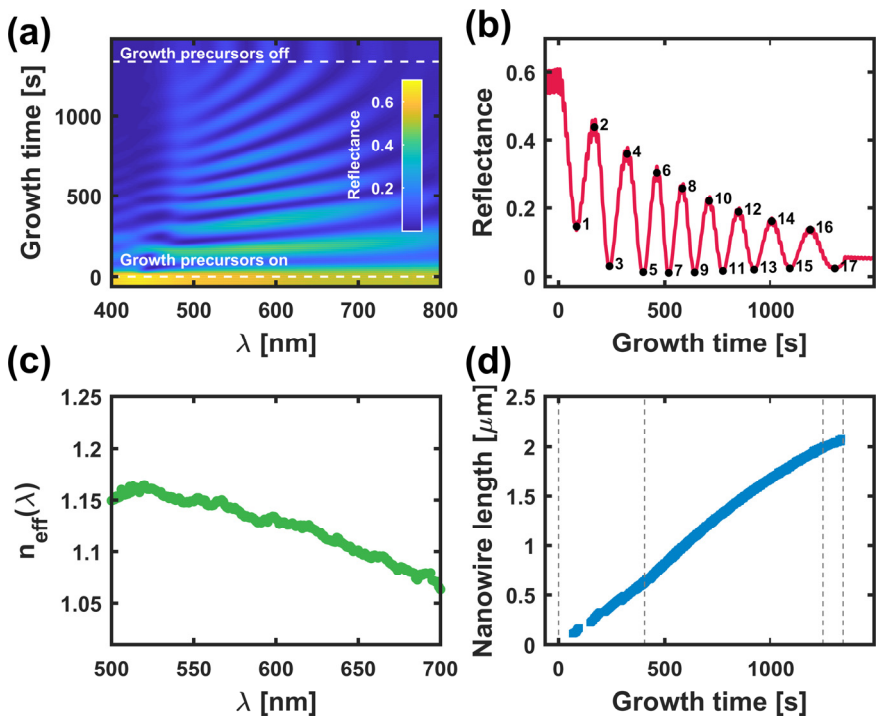


Figure 4.1 In situ growth monitoring by optical reflectometry (**a**) Colorplot of measured reflectance values during growth of an InP nanowire array. (**b**) Reflectance spectrum for light with 550 nm wavelength, equivalent to a line-cut through the data presented in (a). The identified minima and maxima are marked by black circles and numbered as described in the main text. (**c**) Effective refractive index for InP nanowire arrays in the geometry used in this thesis, obtained from calibration runs. (**d**) Nanowire length vs growth time data for InP *p-i-n* nanowires, extracted from the data in (a) by extracting minima and maxima for each wavelength as shown in (b), and using Equation 4.1 together with the effective refractive index in (c). The dashed lines indicate (from left to right); growth start, middle-segment start, top-segment start, and growth end.

Optical reflectometry data as illustrated in Figure 4.1 have been used in a number of different ways in this thesis. First, studying the interference fringes for reference runs have been a first step in detecting any reproducibility issues between growth-sessions and -runs. Second, the real time length monitoring has allowed in situ adjustment of growth times to obtain specific segment lengths. This was used for example in Paper III, IV, VI and IX to grow nanowires for doping evaluation (Chapter 4.3). Here, contact segments of equal length and doping were grown on each side of a middle segment where the dopant molar fraction was varied between runs. The contact segments were highly doped, and facilitated electrical characterization by providing similar contact characteristics between different samples. Lastly, in situ nanowire length data was important in Paper V, where the influence of DEZn on the growth dynamics of $In_xGa_{1-x}P$ nanowires was studied in detail.

For our nanowire arrays, an absorption peak is visible as a dip in the optical reflectance spectrum around 450 nm (Figure 4.1a). This is due to resonant absorption into the diameter dependent HE_{12} waveguide mode [123]. Such diameter dependent absorption resonances in the nanowires are discussed more thoroughly in Paper I. We note here that by monitoring changes in the absorption peak wavelength, evolution of the nanowire diameter can also be monitored in situ, for instance during radial shell growth [123]. This has not been studied in this thesis, but will be useful for example if developing in situ surface passivation of nanowire solar cells.

4.2 Scanning electron microscopy

The first post-growth characterization technique used to inspect the nanowires in this thesis has typically been scanning electron microscopy (SEM). Electron microscopes allow imaging of much smaller structures than an optical microscope, due to the much shorter (typically on the order of 1000×) wavelength of electrons compared to photons. In an SEM, a focused beam of electrons, well defined in energy and flux, is scanned across the sample. By collecting secondary and/or backscattered electrons produced by the beam-sample interaction at each point, a greyscale image is built up where the brightness of each pixel corresponds to the number of collected electrons.

In the work presented in this thesis, SEM has been used extensively to inspect the morphology of the nanowire samples. As illustrative examples we can mention inspection of pattern preservation through stages of nanowire growth (Chapter 3.4.1), nanowire length measurements to calibrate optical reflectometry measurements (Chapter 4.1), and inspection of electron beam lithography defined contacts to single nanowires (Chapter 4.3).

4.3 Doping evaluation

The doping levels in different parts of the solar cell affect performance in important ways, by influencing e.g. the magnitude, extension and position of the built-in electric field, the diffusion lengths in the quasi-neutral regions, and the contact resistances. Therefore, quantitative evaluation of the doping levels in our solar cell material is of central interest. Quantitative doping evaluation of semiconductor nanowires can be done by a number of methods, as thoroughly reviewed by Wallentin and Borgström [115], and discussed briefly in the following.

Historically, the most commonly used doping evaluation method is to make single nanowire FETs [125]. Such a device is typically made by breaking the nanowires off from the growth substrate, dispersing them on a conducting substrate covered with a gate oxide, and defining source and drain contacts to the ends of the nanowire by electron beam lithography (EBL). The charge carrier concentration can be calculated from measured values of the conductivity and mobility, found in the FET nanowire channel by sweeping the source-drain voltage and the gate voltage, respectively. In 2012, a significant achievement was made when the first Hall measurements were reported for nanowires [126, 127]. Here, the simultaneous influence of an electric and magnetic field on the charge carriers in the semiconductor lead to a build-up of a voltage perpendicular to both fields, referred to as the Hall voltage, V_H. By measuring V_H, both the carrier concentration and carrier type can be determined. While using the Hall effect is the standard method to measure carrier concentrations in bulk semiconductors, it was challenging to achieve in the nanowire geometry due to the extreme accuracy needed to position the contacts to measure the Hall voltage.

Besides FET and Hall effect measurements, other notable techniques to quantitatively evaluate doping in semiconductor nanowires include capacitance-voltage (CV) measurements [128], photoluminescence spectroscopy (PL) [129] (Paper VI), cathodoluminescence (CL) [130], Raman spectroscopy [131], and atom-probe tomography [132]. Optical methods such as PL and Raman spectroscopy are interesting as they do not require contacts to be made to the nanowires, while atom probe tomography might provide superior spatial resolution.

In this thesis, the main focus has been on doping evaluation by electrical characterization, in an effort both to evaluate doping levels in nanowires relevant for solar cells, and to develop the characterization techniques themselves. In Paper III, a thorough comparison between charge carrier concentration extraction from Hall and FET measurements was performed on a series of *n*-doped InP nanowires. In these nanowires, degenerate doping was achieved, appropriate for making tunnel diodes (Paper VII). In Paper IV, the same set of nanowires was used to evaluate a measurement design using only one Hall contact as compared to the traditional two. Here, V_H is measured as a potential difference in the single contact with respect to

ground, instead of as a potential difference between two contacts. Using only one contact greatly simplifies the contacting scheme for Hall measurements, and also enables measurement of thinner nanowires than previously possible. Both Hall and FET measurements were used in Paper VI to evaluate *n*-type doping in $In_xGa_{1-x}P$ nanowires, grown with a composition appropriate for nanowire tandem solar cells. As doping might vary both axially and radially in a nanowire, a benefit of using Hall type measurements is the possibility of placing several Hall contacts along the length of the nanowire, obtaining spatial information on the carrier concentration profile, as was done in Paper VI (and Paper IX).

It should be noted that making Ohmic contacts to semiconductors can be challenging, and to nanowires more so [115]. In Paper V, an attempt was made to electrically evaluate *p*-doping in a series of $In_xGa_{1-x}P$ nanowires grown with different DEZn flows. However, all the fabricated single nanowire devices were dominated by poor contact characteristics, preventing accurate assessment of the carrier concentration. Such poor contact characteristics have also been seen in *p*-type InP nanowires [133, 134].

4.4 Electron beam induced current

In Chapter 4.2 we described how the collection of secondary and backscattered electrons resulting from the interaction of a sample with an electron beam can be used to build an SEM image. In addition to this signal, the beam-sample interaction also produces other effects. For example, if the sample has an internal electric field, the electron beam excitation of free carriers within the sample will result in a flow of charge carriers from one region of the sample to another. By contacting the sample, this current can be measured in an external circuit, as an electron beam induced current (EBIC) signal. While the internal electric field may be due to e.g. Schottky contacts or heterointerfaces, the following discussion will be made in terms of fields generated by a *pn*-junction. An excellent review of the fundamentals of the EBIC technique has been given by Leamy [135].

EBIC is a useful technique to characterize solar cell materials [136]. For bulk devices, the sample is for example cleaved or mesa-etched to yield access to a cross-section of the *pn*-junction. By scanning the e-beam across the *pn*-junction and measuring the resulting EBIC signal at each point, an image reflecting the local carrier collection efficiencies can be obtained. This can give information crucial to solar cell performance, such as the location and extension of the depletion region, minority carrier diffusion lengths in the quasi-neutral regions, and effects of e.g. grain boundaries, contacts or surfaces. In bulk solar cells, the surface intersecting the *pn*-junction is introduced to facilitate measurements and might change the charge carrier

collection profiles quite substantially from those in an actually operating solar cell. In contrast, nanowire solar cells inherently have a large surface, and lend themselves well to EBIC characterization.

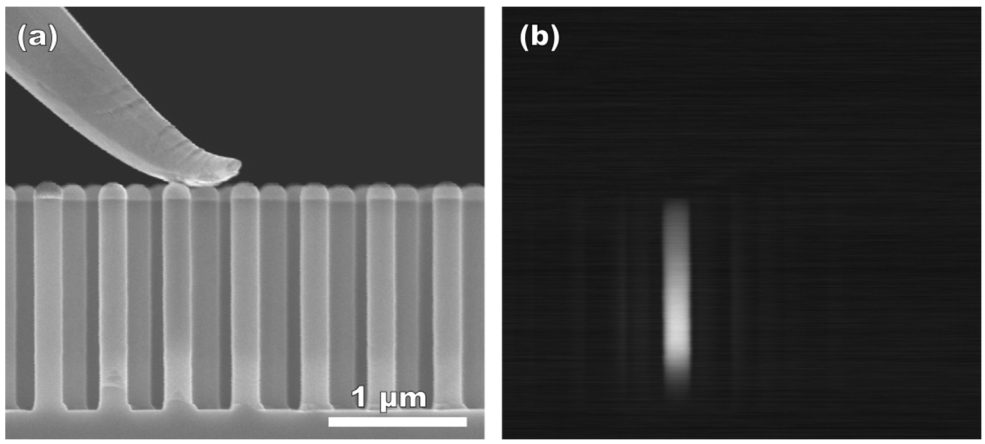


Figure 4.2 Measuring electron beam induced current (EBIC) by help of a nanoprobe inside a scanning electron microscope (SEM). (**a**) Example SEM image of *p-i-n* InP nanowires, where one nanowire is contacted by bringing a tungsten nanoprobe in contact with the gold seed particle. A back contact is provided through the *p*-type growth substrate. (**b**) EBIC signal obtained simultaneously as the SEM image.

Several studies have dealt with EBIC characterization of nanowires broken off and contacted at each end by EBL [134, 137–139]. However, this contacting procedure is fairly time consuming, and as discussed in Chapter 4.3, obtaining good contacts to *p*-type InP and $In_xGa_{1-x}P$ nanowires is challenging. Therefore, for the EBIC characterization in this thesis, a different setup has been used. Here a contact to the *p*-type bottom segment of the nanowires is provided through the *p*-type growth substrate glued to an SEM stub by silver paste. The front contact is made by bringing a tungsten nanoprobe with piezoelectronic positioning control in contact with the gold seed particle on top of a single nanowire. An example SEM image of a contacted sample, and the resulting EBIC signal, is shown in Figure 4.2a and b, respectively.

In Paper VII, we measured EBIC profiles and extracted effective minority carrier diffusion lengths in InP/$In_xGa_{1-x}P$ nanowire heterojunctions, grown with the aim of making tunnel diodes. In Paper VIII, an investigation was done of the carrier collection properties of InP nanowire *p-i-n* junctions, and how these properties related to the growth conditions and the solar cell performance.

4.5 Solar cell *IV*-characteristics

Important parameters describing the performance of a solar cell can be extracted from *IV*-curves. To obtain these, the solar cell is contacted and a bias voltage is swept while measuring the current through the cell. Analyzing *IV*-curves obtained while the solar cell is kept in the dark can give information about the solar cell recombination characteristics (Chapter 2.1.2), while *IV*-curves obtained while the solar cell is illuminated provide the central performance parameters; V_{OC}, J_{SC}, and *FF* (Equation 2.5). The shape of the light *IV*-curve can further give indications about effects on the solar cell performance by e.g. parasitic resistances (Figure 2.6).

In Paper VIII, we obtained *IV* characteristics from single InP nanowires, contacted by a nanoprobe as explained in Chapter 4.4. This allowed us to check dependences of the single nanowire recombination characteristics on different growth parameters. Further, these single nanowire measurements were compared with *IV* characteristics from nanowire solar cells, to reveal effects of the processing conditions on the solar cell performance. Nanowire arrays were processed into 1×1 mm^2 sized solar cells by collaborators at the company SolVoltaics AB, as described in Paper VIII.

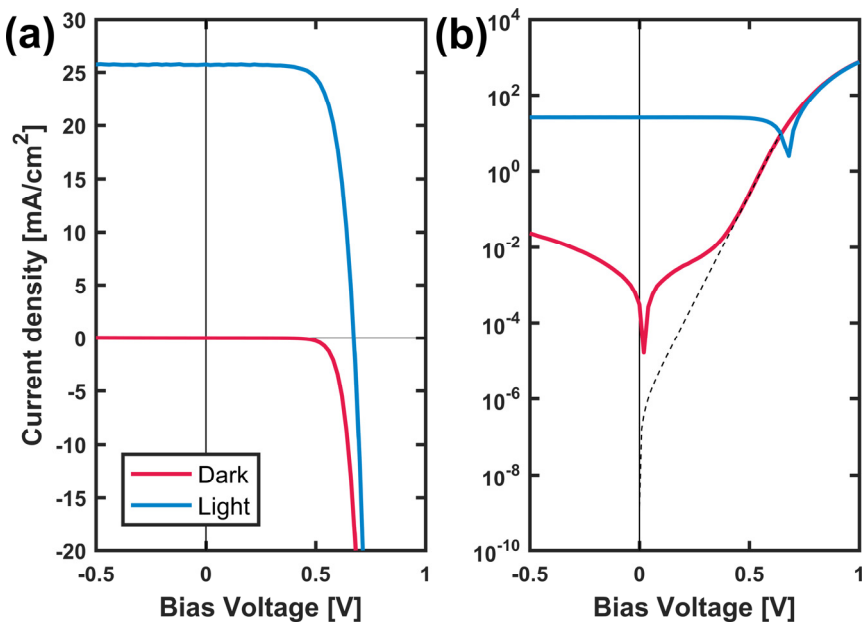


Figure 4.3 Dark and light *IV* data measured for a 1x1 mm^2 InP nanowire solar cell, plotted with a (**a**) linear and (**b**) logarithmic y-axis. In (b), the dashed black line indicate a fit to the single diode equation in the voltage region close to V_{OC}, to obtain values for J_0 and n.

By combining single nanowire EBIC characterization (Chapter 4.4) with *IV*-characterization of both single nanowires and processed solar cells, an improved understanding of the performance of our nanowire solar cells was obtained. We especially studied effects of the shape and position of the EBIC profile on the J_{SC}, as well as effects on recombination of passivating the nanowire sidewalls. This understanding helped us fabricate an InP nanowire solar cell (Figure 4.3), which was measured at Fraunhofer ISE to a certified *PCE* of 15.0%. This is the highest reported value for a bottom-up synthesized InP nanowire solar cell.

5 Summary and outlook

To compete in more than just niche markets, any new solar cell technology will need to reach efficiencies significantly higher than those currently possible with existing single junction Si or thin-film technology [11]. The most likely designs to achieve such efficiencies are the tandem architectures.

For nanowires, one possible tandem design is where different junctions are combined within the same heterostructured nanowire (Figure 2.8a), while another possibility is to place high bandgap nanowires on top of a conventional planar cell (Figure 2.8b). Especially interesting is the possibility to grow or place III-V nanowires on top of conventional Si solar cells, to build on already existing industrial infrastructure. The first such device has already been realized [140], with GaAs nanowires grown directly on top of a Si cell. To further develop such tandem devices, many different pieces of knowledge are needed, relating to synthesis, characterization and device design. A few pieces are provided by this thesis and are summarized in the following.

Although nanowire growth by Aerotaxy seems to have the greatest potential for industrial scale production, the substrate based MOVPE growth used in this thesis is still relevant. Most importantly, these structures are crucial to develop and understand nanowire solar cell characterization, design and performance, as has been attempted in this thesis. Further, MOVPE growth might be the method of choice for tandem structures within the same nanowire, which might be too complex to be achieved with the Aerotaxy technique. For MOVPE growth of such structures to be cost-effective one should grow on a cheap foreign substrate and/or develop good methods for substrate reuse. The techniques used for substrate patterning and pattern preservation on native substrates in this thesis are relevant also for other substrates. Additionally, this thesis provides some of the first systematic studies on the effects of doping on ternary III-V nanowire growth. This knowledge was used to realize and study the first nanowire tunnel junction connecting two materials of appropriate bandgaps to match the solar spectrum.

In addition to the experimental work, the thesis organizes and summarizes current knowledge about benefits, challenges and design guidelines when making nanowire solar cells. This resulted in a review paper (Paper I), providing an accessible source of information for other researchers.

Going forward, a number of potential improvements for the InP nanowire solar cells presented in Paper VIII will be interesting to explore. For example, the passivation of the surface needs to be further improved and understood. With a well-passivated surface, further optimization of nanowire doping and segment lengths should be possible. Also, modelling has predicted that replacing the top n-segment with a non-absorbing GaP segment will give a boost to the J_{SC} [141]. Further, the fairly high series resistance in the devices reported in Paper VIII indicates that there is potential for improving the top contact. Additionally, if long enough diffusion lengths in the material are obtained, one could potentially remove the intrinsic middle segment, which should help improve the V_{OC}. Finally, expanding the current single-junction InP cell into a double-junction InP/$In_xGa_{1-x}P$ nanowire solar cell is a highly interesting and challenging project, for which most building blocks are now in place.

Important to note is that if III-V nanowire solar cells are to become a commercial alternative, proper life-cycle analysis of environmental impacts needs to be performed. This should if needed result in the development of adequate methods for encapsulation, handling and/or recycling of the materials. Further, the cells need to be rigorously tested in terms of reliability and stability in the field.

Lastly, it should be noted that much of the knowledge established through this thesis work is relevant also to other applications of III-V nanowires, such as nanowire photodetectors or LEDs.

References

1. IPCC, *Climate Change 2014 - Synthesis report* (Cambridge University Press, Cambridge, 2014), doi:10.1017/CBO9781107415324.
2. Lee, R., *The Outlook for Population Growth*. Science. **333** (2011) p. 569–573.
3. United Nations, *Sustainable development goals: Poverty*, (available at http://www.un.org/sustainabledevelopment/poverty/).
4. Chu, S., Majumdar, A., *Opportunities and challenges for a sustainable energy future.* Nature. **488** (2012) p. 294–303.
5. ©*Fraunhofer ISE: Photovoltaics Report, updated 12 July 2017* (2017), (available at https://www.ise.fraunhofer.de/en/renewable-energy-data).
6. Breyer, C., Gerlach, A., *Global overview on grid-parity*. Prog. Photovoltaics Res. Appl. **21** (2013) p. 121–136.
7. ©*Fraunhofer ISE: Photovoltaics Report, updated 6 June 2016* (2016), (available at https://www.ise.fraunhofer.de/en/renewable-energy-data).
8. IEA (International Energy Agency), *Next Generation Wind and Solar Power* (2016), doi:10.1787/9789264258969-en.
9. Lewis, N. S., *Research opportunities to advance solar energy utilization*. Science. **351** (2016) doi:10.1126/science.aad1920.
10. Polman, A. et al., *Photovoltaic materials: Present efficiencies and future challenges*. Science. **352** (2016) doi:10.1126/science.aad4424.
11. Green, M. A., *Commercial progress and challenges for photovoltaics*. Nat. Energy. **1** (2016) p. 15015.
12. Yoshikawa, K. et al., *Silicon heterojunction solar cell with interdigitated back contacts for a photoconversion efficiency over 26%*. Nat. Energy. **2** (2017) p. 17032.
13. Richter, A., Hermle, M., Glunz, S. W., *Reassessment of the Limiting Efficiency for Crystalline Silicon Solar Cells*. IEEE J. Photovoltaics. **3** (2013) p. 1184–1191.
14. Green, M. A., Bremner, S. P., *Energy conversion approaches and materials for high-efficiency photovoltaics*. Nat. Mater. **16** (2017) p. 23–34.
15. Tsakalakos, L., *Nanostructures for photovoltaics*. Mater. Sci. Eng. R Reports. **62** (2008) p. 175–189.
16. Beard, M. C., Luther, J. M., Nozik, A. J., *The promise and challenge of nanostructured solar cells*. Nat. Nanotechnol. **9** (2014) p. 951–954.

17. Dasgupta, N. P. et al., *25th anniversary article: Semiconductor nanowires - Synthesis, characterization, and applications*. Adv. Mater. **26** (2014) p. 2137–2183.

18. Huynh, W. U., Dittmer, J. J., Alivisatos, A. P., *Hybrid Nanorod-Polymer Solar Cells*. Science. **295** (2002) p. 2425–2427.

19. Law, M. et al., *Nanowire dye-sensitized solar cells*. Nat. Mater. **4** (2005) p. 455–459.

20. Baxter, J. B., Aydil, E. S., *Nanowire-based dye-sensitized solar cells*. Appl. Phys. Lett. **86** (2005) p. 53114.

21. Song, M. Y. et al., *TiO2 single-crystalline nanorod electrode for quasi-solid-state dye-sensitized solar cells*. Appl. Phys. Lett. **87** (2005) p. 113113.

22. Tian, B. et al., *Coaxial silicon nanowires as solar cells and nanoelectronic power sources*. Nature. **449** (2007) p. 885–889.

23. Kelzenberg, M. D. et al., *Photovoltaic measurements in single-nanowire silicon solar cells*. Nano Lett. **8** (2008) p. 710–714.

24. Czaban, J. A., Thompson, D. A., LaPierre, R. R., *GaAs core- shell nanowires for photovoltaic applications*. Nano Lett. **9** (2008) p. 148–154.

25. Colombo, C., Heiss, M., Grätzel, M., Fontcuberta i Morral, A., *Gallium arsenide p-i-n radial structures for photovoltaic applications*. Appl. Phys. Lett. **94** (2009) p. 173108.

26. Goto, H. et al., *Growth of core-shell InP nanowires for photovoltaic application by selective-area metal organic vapor phase epitaxy*. Appl. Phys. Express. **2** (2009) p. 35004.

27. Åberg, I. et al., *A GaAs Nanowire Array Solar Cell With 15.3% Efficiency at 1 Sun*. IEEE J. Photovoltaics. **6** (2016) p. 185–190.

28. van Dam, D. et al., *High-Efficiency Nanowire Solar Cells with Omnidirectionally Enhanced Absorption Due to Self-Aligned Indium–Tin–Oxide Mie Scatterers*. ACS Nano. **10** (2016) p. 11414–11419.

29. Gray, J. L., in *Handbook of Photovoltaic Science and Engineering*, A. L. and S. Hegedus, Ed. (John Wiley & Sons, Ltd, ed. 1, 2003), pp. 61–112.

30. *Solar Spectra: ASTM G-173. NREL's Power Syst. Eng. Cent.*, (available at http://rredc.nrel.gov/solar/spectra/).

31. Shockley, W., Queisser, H. J., *Detailed Balance Limit of Efficiency of p-n Junction Solar Cells*. J. Appl. Phys. **32** (1961) p. 510–519.

32. Green, M. A. et al., *Solar cell efficiency tables (version 50)*. Prog. Photovoltaics Res. Appl. **25** (2017) p. 668–676.

33. Ross, R. T., Nozik, A. J., *Efficiency of hot-carrier solar energy converters*. J. Appl. Phys. **53** (1982) p. 3813–3818.

34. Trupke, T., Green, M. A., Würfel, P., *Improving solar cell efficiencies by down-conversion of high-energy photons*. J. Appl. Phys. **92** (2002) p. 1668–1674.

35. Luque, A., Martí, A., Stanley, C., *Understanding intermediate-band solar cells*. Nat. Photonics. **6** (2012) p. 146–152.

36. Semonin, O. E., Luther, J. M., Beard, M. C., *Quantum dots for next-generation photovoltaics*. Mater. Today. **15** (2012) p. 508–515.

37. Olson, J. M., Friedman, D. J., Kurtz, S., in *Handbook of Photovoltaic Science and Engineering*, A. Luque, S. Hegedus, Eds. (John Wiley & Sons, Ltd, ed. 1, 2003), pp. 359–411.

38. Green, M. A., in *Third Generation Photovoltaics* (Springer, New York, 2006), pp. 59–67.

39. Araújo, G. L., Martí, A., *Absolute limiting efficiencies for photovoltaic energy conversion*. Sol. Energy Mater. Sol. Cells. **33** (1994) p. 213–240.

40. Würfel, P., *Thermodynamic limitations to solar energy conversion*. Phys. E Low-Dimensional Syst. Nanostructures. **14** (2002) p. 18–26.

41. Green, M. A., *Third generation photovoltaics* (Springer, New York, 2006).

42. Martí, A., Balenzategui, J. L., Reyna, R. F., *Photon recycling and Shockley's diode equation*. J. Appl. Phys. **82** (1997) p. 4067–4075.

43. Polman, A., Atwater, H. A., *Photonic design principles for ultrahigh-efficiency photovoltaics*. Nat. Mater. **11** (2012) p. 174–177.

44. Ptak, A. J., Friedman, D. J., Kurtz, S., Reedy, R. C., *Low-acceptor-concentration GaInNAs grown by molecular-beam epitaxy for high-current p-i-n solar cell applications*. J. Appl. Phys. **98** (2005) p. 94501.

45. Cuevas, A., *The recombination parameter J0*. Energy Procedia. **55** (2014) p. 53–62.

46. Breitenstein, O., Rakotoniaina, J. P., Al Rifai, M. H., Werner, M., *Shunt types in crystalline silicon solar cells*. Prog. Photovoltaics Res. Appl. **12** (2004) p. 529–538.

47. Anttu, N., Xu, H. Q., *Efficient light management in vertical nanowire arrays for photovoltaics*. Opt. Express. **21** (2013) p. A558.

48. Wanlass, M., *Systems and methods for advanced ultra-high-performance InP solar cells (US Patent)* (2017).

49. Glas, F., *Critical dimensions for the plastic relaxation of strained axial heterostructures in free-standing nanowires*. Phys. Rev. B. **74** (2006) p. 121302.

50. Spurgeon, J. M. et al., *Repeated epitaxial growth and transfer of arrays of patterned, vertically aligned, crystalline Si wires from a single Si(111) substrate*. Appl. Phys. Lett. **93** (2008) p. 32112.

51. Chen, M., Nakai, E., Tomioka, K., Fukui, T., *Application of free-standing InP nanowire arrays and their optical properties for resource-saving solar cells*. Appl. Phys. Express. **8** (2015) p. 12301.

52. Heurlin, M. et al., *Continuous gas-phase synthesis of nanowires with tunable properties*. Nature. **492** (2012) p. 90–94.

53. Barrigon, E. et al., *GaAs nanowire pn-junctions produced by low-cost and high-throughput Aerotaxy*. Nano Lett. (2017) doi:10.1021/acs.nanolett.7b04609.

54. Anttu, N., *Shockley–Queisser Detailed Balance Efficiency Limit for Nanowire Solar Cells*.

ACS Photonics. **2** (2015) p. 446–453.

55. Xu, Y., Gong, T., Munday, J. N., *The generalized Shockley-Queisser limit for nanostructured solar cells*. Sci. Rep. **5** (2015) p. 13536.

56. Mann, S. A. et al., *Opportunities and Limitations for Nanophotonic Structures To Exceed the Shockley–Queisser Limit*. ACS Nano. **10** (2016) p. 8620–8631.

57. Wallentin, J. et al., *InP Nanowire Array Solar Cells Achieving 13.8% Efficiency by Exceeding the Ray Optics Limit.* Science. **339** (2013) p. 1057–1060.

58. Cho, K. et al., *Molecular monolayers for conformal, nanoscale doping of InP nanopillar photovoltaics*. Appl. Phys. Lett. **98** (2011) p. 203101.

59. Dhindsa, N. et al., *Highly ordered vertical GaAs nanowire arrays with dry etching and their optical properties*. Nanotechnology. **25** (2014) p. 305303.

60. Stringfellow, G. B., in *Organometallic Vapor-Phase Epitaxy: Theory and Practice* (Academic Press, 1999), pp. 151–209.

61. Stringfellow, G. B., in *Organometallic Vapor-Phase Epitaxy: Theory and Practice1* (Academic Press, 1999), pp. 211–295.

62. Pohl, U. W., *Epitaxy of Semiconductors* (Springer Verlag, Berlin, Heidelberg, 2013).

63. Stringfellow, G. B., in *Organometallic Vapor-Phase Epitaxy: Theory and Practice* (Academic Press, 1999), pp. 364–384.

64. Greiner, E. S., Gutowski, J. A., Ellis, W. C., *Preparation of silicon ribbons*. J. Appl. Phys. **32** (1961) p. 2489–2490.

65. Wagner, R. S., Ellis, W. C., Jackson, K. A., Arnold, S. M., *Study of the filamentary growth of silicon crystals from the vapor*. J. Appl. Phys. **35** (1964) p. 2993–3000.

66. Wagner, R. S., Ellis, W. C., *VAPOR-LIQUID-SOLID MECHANISM OF SINGLE CRYSTAL GROWTH*. Appl. Phys. Lett. **4** (1964) p. 89–90.

67. Dick, K. A., *A review of nanowire growth promoted by alloys and non-alloying elements with emphasis on Au-assisted III-V nanowires*. Prog. Cryst. Growth Charact. Mater. **54** (2008) p. 138–173.

68. Wacaser, B. A. et al., *Preferential interface nucleation: An expansion of the VLS growth mechanism for nanowires*. Adv. Mater. **21** (2009) p. 153–165.

69. Persson, A. I. et al., *Solid-phase diffusion mechanism for GaAs nanowire growth.* Nat. Mater. **3** (2004) p. 677–81.

70. Kodambaka, S., Tersoff, J., Reuter, M. C., Ross, F. M., *Germanium nanowire growth below the eutectic temperature.* Science. **316** (2007) p. 729–32.

71. Dong, A., Wang, F., Daulton, T. L., Buhro, W. E., *Solution-liquid-solid (SLS) growth of ZnSe-ZnTe quantum wires having axial heterojunctions*. Nano Lett. **7** (2007) p. 1308–1313.

72. Dick, K. A., Caroff, P., *Metal-seeded growth of III – V semiconductor nanowires : towards gold-free synthesis*. Nanoscale. **6** (2014) p. 3006–3021.

73. Colombo, C. et al., *Ga-assisted catalyst-free growth mechanism of GaAs nanowires by molecular beam epitaxy*. Phys. Rev. B. **77** (2008) p. 155326.

74. Verheijen, M. A. et al., *Growth kinetics of heterostructured GaP-GaAs nanowires*. J. Am. Chem. Soc. **128** (2006) p. 1353–1359.

75. Kodambaka, S., Tersoff, J., Reuter, M. C., Ross, F. M., *Diameter-independent kinetics in the vapor-liquid-solid growth of Si nanowires*. Phys. Rev. Lett. **96** (2006) p. 1–4.

76. Borgström, M. T. et al., *Synergetic nanowire growth.* Nat. Nanotechnol. **2** (2007) p. 541–544.

77. Glas, F., Harmand, J.-C., Patriarche, G., *Why Does Wurtzite Form in Nanowires of III-V Zinc Blende Semiconductors?* Phys. Rev. Lett. **99** (2007) p. 146101.

78. Glas, F., Harmand, J. C., Patriarche, G., *Nucleation antibunching in catalyst-assisted nanowire growth*. Phys. Rev. Lett. **104** (2010) p. 2–5.

79. Dubrovskii, V. G., *Nucleation Theory and Growth of Nanostructures* (Springer Berlin Heidelberg, Berlin, Heidelberg, 2014; http://link.springer.com/10.1007/978-3-642-39660-1), *NanoScience and Technology*.

80. Mårtensson, T. et al., *Epitaxial III–V Nanowires on Silicon*. Nano Lett. **4** (2004) p. 1987–1990.

81. Bakkers, E. P. A. M., Borgström, M. T., Verheijen, M. A., *Epitaxial Growth of III – V Nanowires on Group IV Substrates*. MRS Bull. **32** (2007) p. 117–122.

82. Ikejiri, K., Ishizaka, F., Tomioka, K., Fukui, T., *GaAs nanowire growth on polycrystalline silicon thin films using selective-area MOVPE.* Nanotechnology. **24** (2013) p. 115304.

83. Borg, M. et al., *Vertical III-V nanowire device integration on Si(100)*. Nano Lett. **14** (2014) p. 1914–1920.

84. Munshi, A. M. et al., *Vertically aligned GaAs nanowires on graphite and few-layer graphene: Generic model and epitaxial growth*. Nano Lett. **12** (2012) p. 4570–4576.

85. Hong, Y. J. et al., *Van der Waals epitaxy of InAs nanowires vertically aligned on single-layer graphene*. Nano Lett. **12** (2012) p. 1431–1436.

86. Wallentin, J., Kriegner, D., Stangl, J., Borgström, M. T., *Au-Seeded Growth of Vertical and in-Plane III–V Nanowires on Graphite Substrates*. Nano Lett. **14** (2014) p. 1707–1713.

87. Gudiksen, M. S. et al., *Growth of nanowire superlattice structures for nanoscale photonics and electronics.* Nature. **415** (2002) p. 617–620.

88. Dhaka, V. et al., *High Quality GaAs Nanowires Grown on Glass Substrates*. Nano Lett. **12** (2012) p. 1912–1918.

89. Cohin, Y. et al., *Growth of vertical GaAs nanowires on an amorphous substrate via a fiber-textured Si platform*. Nano Lett. **13** (2013) p. 2743–2747.

90. Fortuna, S. A., Li, X., *Metal-catalyzed semiconductor nanowires: a review on the control of growth directions*. Semicond. Sci. Technol. **25** (2010) p. 24005.

91. Fan, H. J., Werner, P., Zacharias, M., *Semiconductor nanowires: From self-organization to patterned growth*. Small. **2** (2006) p. 700–717.

92. Messing, M. E. et al., *A comparative study of the effect of gold seed particle preparation method on nanowire growth*. Nano Res. **3** (2010) p. 506–519.

93. Mårtensson, T. et al., *Fabrication of individually seeded nanowire arrays by vapour-liquid-solid growth*. Nanotechnology. **14** (2003) p. 1255–1258.

94. Kim, D. S. et al., *Laser-interference lithography tailored for highly symmetrically arranged ZnO nanowire arrays*. Small. **3** (2007) p. 76–80.

95. Kauppinen, C. et al., *A technique for large-area position-controlled growth of GaAs nanowire arrays*. Nanotechnology. **27** (2016) p. 135601.

96. Fuhrmann, B. et al., *Ordered arrays of silicon nanowires produced by nanosphere lithography and molecular beam epitaxy.* Nano Lett. **5** (2005) p. 2524–2527.

97. Madaria, A. R. et al., *Toward optimized light utilization in nanowire arrays using scalable nanosphere lithography and selected area growth*. Nano Lett. **12** (2012) p. 2839–2845.

98. Solak, H. H., Dais, C., Clube, F., *Displacement Talbot lithography: a new method for high-resolution patterning of large areas.* Opt. Express. **19** (2011) p. 10686–10691.

99. Chou, S. Y., Krauss, P. R., Renstrom, P. J., *Imprint of sub-25 nm vias and trenches in polymers*. Appl. Phys. Lett. **67** (1995) p. 3114.

100. Chou, S. Y., Krauss, P. R., Renstrom, P. J., *Imprint Lithography with 25-Nanometer Resolution*. Science. **272** (1996) p. 85–87.

101. Traub, M. C., Longsine, W., Truskett, V. N., *Advances in Nanoimprint Lithography*. Annu. Rev. Chem. Biomol. Eng. **7** (2016) p. 583–604.

102. Mårtensson, T. et al., *Nanowire arrays defined by nanoimprint lithography*. Nano Lett. **4** (2004) p. 699–702.

103. Eriksson, T. et al., *High volume nanoimprint lithography on III/V substrates: Imprint fidelity and stamp lifetime*. Microelectron. Eng. **88** (2011) p. 293–299.

104. Pierret, A. et al., *Generic nano-imprint process for fabrication of nanowire arrays.* Nanotechnology. **21** (2010) p. 65305.

105. Cavalli, A. et al., *Influence of growth conditions on the performance of InP nanowire solar cells*. Nanotechnology. **27** (2016) p. 454003.

106. Jacobsson, D. et al., *Interface dynamics and crystal phase switching in GaAs nanowires*. Nature. **531** (2016) p. 317–322.

107. Wallentin, J. et al., *Electron trapping in InP nanowire FETs with stacking faults*. Nano Lett. **12** (2012) p. 151–155.

108. Johansson, J. et al., *Structural properties of 〈111〉 B -oriented III–V nanowires*. Nat. Mater. **5** (2006) p. 574–580.

109. Caroff, P. et al., *Controlled polytypic and twin-plane superlattices in III-V nanowires.*

Nat. Nanotechnol. **4** (2009) p. 50–55.

110. Joyce, H. J. et al., *High purity GaAs nanowires free of planar defects: Growth and characterization*. Adv. Funct. Mater. **18** (2008) p. 3794–3800.

111. Algra, R. E. et al., *The Role of Surface Energies and Chemical Potential during Nanowire Growth*. Nano Lett. **11** (2011) p. 1259–1264.

112. Krogstrup, P. et al., *Impact of the Liquid Phase Shape on the Structure of III-V Nanowires*. Phys. Rev. Lett. **106** (2011) p. 125505.

113. Algra, R. E. et al., *Twinning superlattices in indium phosphide nanowires*. Nature. **456** (2008) p. 369–372.

114. Wallentin, J. et al., *Changes in contact angle of seed particle correlated with increased zincblende formation in doped InP nanowires.* Nano Lett. **10** (2010) p. 4807–12.

115. Wallentin, J., Borgström, M. T., *Doping of semiconductor nanowires*. J. Mater. Res. **26** (2011) p. 2142–2156.

116. Björk, M. T. et al., *One-dimensional Steeplechase for Electrons Realized*. Nano Lett. **2** (2002) p. 87–89.

117. Wu, Y., Fan, R., Yang, P., *Block-by-Block Growth of Single-Crystalline Si/SiGe Superlattice Nanowires*. Nano Lett. **2** (2002) p. 83–86.

118. Kuech, T. F. et al., *The control and modeling of doping profiles and transients in MOVPE growth*. J. Cryst. Growth. **93** (1988) p. 624–630.

119. Borgström, M. T. et al., *Interface study on heterostructured GaP–GaAs nanowires*. Nanotechnology. **17** (2006) p. 4010–4013.

120. Dick, K. A., Bolinsson, J., Borg, B. M., Johansson, J., *Controlling the abruptness of axial heterojunctions in III-V nanowires: Beyond the reservoir effect*. Nano Lett. **12** (2012) p. 3200–3206.

121. Borgström, M. T. et al., *In situ etching for total control over axial and radial nanowire growth*. Nano Res. **3** (2010) p. 264–270.

122. Berg, A. et al., *In situ etching for control over axial and radial III-V nanowire growth rates using HBr*. Nanotechnology. **25** (2014) p. 505601.

123. Heurlin, M. et al., *In Situ Characterization of Nanowire Dimensions and Growth Dynamics by Optical Reflectance*. Nano Lett. **15** (2015) p. 3597–3602.

124. Heurlin, M., *Nanowire Growth Analysis v.1.3 (Matlab program)* (2016).

125. Cui, Y., Duan, X., Hu, J., Lieber, C. M., *Doping and Electrical Transport in Silicon Nanowires*. J. Phys. Chem. B. **104** (2000) p. 5213–5216.

126. Storm, K. et al., *Spatially resolved Hall effect measurement in a single semiconductor nanowire.* Nat. Nanotechnol. **7** (2012) p. 718–22.

127. Blömers, C. et al., *Hall effect measurements on InAs nanowires*. Appl. Phys. Lett. **101** (2012) p. 152106.

128. Garnett, E. C. et al., *Dopant profiling and surface analysis of silicon nanowires using*

capacitance-voltage measurements. Nat. Nanotechnol. **4** (2009) p. 311–314.

129. Liu, C. et al., *Blueshift of electroluminescence from single n-InP nanowire/p-Si heterojunctions due to the Burstein-Moss effect.* Nanotechnology. **19** (2008) p. 465203.

130. Lindgren, D. et al., *Study of carrier concentration in single InP nanowires by luminescence and Hall measurements.* Nanotechnology. **26** (2015) p. 45705.

131. Hilse, M. et al., *Incorporation of the dopants Si and Be into GaAs nanowires*. Appl. Phys. Lett. **96** (2010) p. 2008–2011.

132. Perea, D. E. et al., *Direct measurement of dopant distribution in an individual vapour-liquid-solid nanowire.* Nat. Nanotechnol. **4** (2009) p. 315–319.

133. Borgström, M. T. et al., *Nanowires with promise for photovoltaics*. IEEE J. Sel. Top. Quantum Electron. **17** (2011) p. 1050–1061.

134. Wallentin, J. et al., *Degenerate p-doping of InP nanowires for large area tunnel diodes*. Appl. Phys. Lett. **99** (2011) p. 253105.

135. Leamy, H. J., *Charge collection scanning electron microscopy*. J. Appl. Phys. **53** (1982) p. R51–R80.

136. Durose, K. et al., *Physical characterization of thin-film solar cells*. Prog. Photovoltaics Res. Appl. **12** (2004) p. 177–217.

137. Allen, J. E. et al., *High-resolution detection of Au catalyst atoms in Si nanowires.* Nat. Nanotechnol. **3** (2008) p. 168–173.

138. Gutsche, C. et al., *Direct determination of minority carrier diffusion lengths at axial GaAs nanowire p-n junctions*. Nano Lett. **12** (2012) p. 1453–1458.

139. Chang, C.-C. et al., *Electrical and Optical Characterization of Surface Passivation in GaAs Nanowires*. Nano Lett. **12** (2012) p. 4484–4489.

140. Yao, M. et al., *Tandem Solar Cells Using GaAs Nanowires on Si: Design, Fabrication, and Observation of Voltage Addition*. Nano Lett. **15** (2015) p. 7217–7224.

141. Chen, Y., Kivisaari, P., Pistol, M.-E., Anttu, N., *Optimization of the short-circuit current in an InP nanowire array solar cell through opto-electronic modeling*. Nanotechnology. **27** (2016) p. 435404.

142. Luo, X., Wang, J., Dooner, M., Clarke, J., *Overview of current development in electrical energy storage technologies and the application potential in power system operation*. Appl. Energy. **137** (2015) p. 511–536.

143. Limpert, S. et al., *Single-nanowire, low-bandgap hot carrier solar cells with tunable open-circuit voltage*. Nanotechnology. **28** (2017) p. 434001.